Solid-State Nuclear Magnetic Resonance Investigation on Crystallization of Xonotlite from Poorly-Crystalline Calcium Silicate Hydrate (C-S-H)

野間, 弘昭
九州大学理学研究科化学専攻

https://doi.org/10.11501/3134917

出版情報：九州大学, 1997, 博士（理学）, 課程博士
バージョン：
権利関係：

Solid-State Nuclear Magnetic Resonance Investigation on Crystallization of Xonotlite from Poorly-Crystalline Calcium Silicate Hydrate (C-S-H)

長 間 弘 昭

Solid-State Nuclear Magnetic Resonance Investigation on Crystallization of Xonotlite from Poorly-Crystalline Calcium Silicate Hydrate (C-S-H)

By
Hiroaki Noma

March, 1998

Department of Chemistry, Faculty of Science
Kyushu University

Table of Contents

Abbreviations

CP	Cross Polarization
CP-MAS	Cross Polarization with MAS
HD	High Power Decoupling
HD-MAS	High Power Decoupling with MAS
C-S-H	Poorly Crystalline Calcium Silicate Hydrates
MAS	Magic Angle Spinning
NMR	Nuclear Magnetic Resonance
ppm	part par million
SEM	Scanning Electron Microscope
TEM	Transmission Electron Microscope
TMS	Trimethylsilyl Silane (standard for ^{29}Si and ^{1}H NMR)
TG	Thermogravimetry
XRD	X-ray Diffraction

Chapter 1

Introduction

1. 1 Calcium Silicate Hydrates

The CaO-SiO_2-H_2O system has around 25 kinds of crystalline calcium silicate hydrates [1, 2]. Among them 21 kinds of the calcium silicate hydrates exist in nature and most of them have been hydrothermally synthesized. In particular, 1.1 nm tobermorite $[Ca_4(Si_3O_9H)_2]Ca.4H_2O$ and xonotlite $[Ca_6(Si_6O_{17})(OH)_2]$ are industrially produced by hydrothermal synthesis around at 200 °C and utilized as building materials and thermal insulators. Moreover, there is a group of poorly crystalline calcium silicate hydrates, which is called C-S-H. The C-S-H is the main component of cement hydration products which bind concrete structure. Therefore, the calcium silicate hydrate is the most important material in the cement chemistry.

1. 2 Xonotlite

Xonotlite $[Ca_6(Si_6O_{17})(OH)_2]$ is named after Xonotla, a place name in Mexico. This is relatively abundant in nature among the calcium silicate hydrates and hydrothermally synthesized below 250 °C under saturated steam pressure. The first well established synthesis was by Nagai [3, 4].

Xonotlite decomposes topotactically to wollastonite [β-$CaSiO_3$] at about 700 °C [5, 6] and its volume change is so small that xonotlite can be used up to 1000 °C as a building material. Xonotlite forms prismatic crystals or fibrous aggregates with elongation parallel to *b*. This fibrous aggregate makes a porous structure. Utilizing the heat resistant property and the porous structure of the aggregate of xonotlite crystals,

a high-performance thermal insulating material was developed in Japan and has been produced.

The crystal structure was determined by Mamedov and Belov [7] who found that dreier double chains of empirical formula $(Si_6O_{17})^{12-}$ were present, together with Ca^{2+} and OH^- ions. Figure 1.1 shows the one of these dreier double chains. Mamedov and Belov concluded from their X-ray study that the formula of xonotlite is $Ca_6(Si_6O_{17})(OH)_2$. Kalousek et al. [8] analyzed 15 natural and synthetic xonotlites by the cell parameters, thermogravimetry and analytical electron microscopy. They concluded that xonotlite tends to be defective in Ca, charge balance being maintained by incorporation of additional H atoms, which are attached to silicate anion. This tendency increases as the temperature of preparation decreases. Gard reported several polytypic variants in xonotlite crystals by electron-diffraction study [9]. Kudoh and Takéuchi [10] determined the exact crystal structure of xonotlite by X-ray diffraction and discussed the polytypism of xonotlite, which is of particular interest because its polytypic variants may occur in such a way that they vary both *a* and *c* periodicities, whereas wollastonite only the periodicity of *a*. The structure of xonotlite determined by Kudoh and Takéuchi [10] is shown in Figure 1.2.

1.3 Formation of Xonotlite

Xonotlite is hydrothermally synthesized below 250 °C under saturated steam pressure. Mitsuda et al. [11] studied the variation in the reaction sequence and kinetics by using several starting materials with Ca/Si = 1.0 of xonotlite composition in stirred suspension at 180 °C. They clarified that the formation of xonotlite from lime - silica mixtures proceeds through intermediate phases such as C-S-H (poorly crystalline calcium silicate hydrate), α-C_2SH (dicalcium silicate hydrate) and tobermorite [11]. When quartz was used as siliceous materials, Ca-rich C-S-H was formed in the early stage before quartz did not completely reacted, then tobermorite was formed from the C-S-H as an intermediate phase and finally xonotlite was formed. While C-S-H formed from amorphous silica directly changed to xonotlite.

In order to explain the slowness of tobermorite formation from the C-S-H using amorphous silica, they suggested two explanations [12]. One is that the higher

concentration of silica in reaction solution may inhibit the tobermorite formation. Another is that a type of C-S-H is structurally less readily converted into tobermorite. They suggested the above explanations but these were not proved. The C-S-H is poorly crystalline and shows only a few broad XRD peaks. The Ca/Si composition of C-S-H varies from 0.5 to 1.7 but there is no clear difference in XRD patterns. This inhibited the characterization of C-S-H.

The studies of the hydrothermal reaction kinetics of calcium silicate hydrates, including xonotlite, tobermorite and so forth, are very few. The reaction proceeds in an autoclave under high pressure and high temperatures, which causes experimental difficulty. The reaction proceeds through intermediate phases, which makes the reaction system complex. Quantitative analysis of the reaction products by XRD is also difficult because XRD peaks of C-S-H overlapped those of the produced crystals.

Kondo et al. [13] first made the quantitative kinetic study of hydrothermal reaction between lime and silica. In this study the reactivity of silica glass and quartz in molded cylindrical specimens was compared. He defined the reaction conversion, α, as

$$\alpha = (\text{combined CaO} + \text{combined } SiO_2)/ (\text{total CaO} + \text{total } SiO_2),$$

and applied the following reaction kinetics

$$(1 - (1 - \alpha)^{1/3})^N = k t^{1/2} .$$

According to the value of the reaction index, N, he considered that N of 1 indicates that the reaction was dissolution-controlled and that N of 2 indicates diffusion-controlled.

Chan et al. [14], Ishii et al. [15] and Mitsuda et al. [11] applied this Kondo's method to the suspension hydrothermal system of CaO and quartz and concluded that the reaction was controlled by dissolution of quartz and lime.

I considered that the problem is that the above analysis of the reaction is treating only the total reaction though the reaction is a multistep reaction and proceeds from CaO and SiO_2 through intermediate phases to the final products. C-S-H seems to be formed by the dissolution of CaO and silica according to the preceding works [13, 14, 15]. But the formation mechanism of xonotlite from C-S-H is still unclear: **where dose the nucleation occur and the crystal glow?**

1.4 Poorly-Crystalline Calcium Silicate Hydrate (C-S-H)

C-S-H is a general term of poorly crystalline calcium silicate hydrates. C-S-H has a wide range of Ca/Si molar ratios between 0.5 and 1.7 and shows only a few broad XRD peaks [16].

The C-S-H phases can be divided into two categories: very poorly crystalline phase and quasi-crystalline phases. The very poorly crystalline phase is called C-S-H gel. The C-S-H gel [17, 18] is a main product of reaction of Portland cement with water at ordinary temperature. The quasi-crystalline phases are divided into two phases, C-S-H(I) and C-S-H(II) by Taylor [17, 18, 19, 20].

The C-S-H(I) has a Ca/Si molar ratio less than 1.5, while the C-S-H(II) has a Ca/Si molar ratio greater than 1.5. Taylor first proposed that a clay-like layer structure for both C-S-H(I) and C-S-H(II) in 1950 [19]. Bernal [21] suggested that the layer structure be related to that of 1.1 nm tobermorite $[Ca_4(Si_3O_9H)_2]Ca.4H_2O$. Later, Taylor and his colleagues proposed that C-S-H(I) has a structure similar to that of 1.4 nm tobermorite $[Ca_4(Si_3O_9H)_2]Ca.8H_2O$ and C-S-H(II) has a structure similar to that of jennite $Ca_8(Si_3O_9H)_2(OH)_8]Ca.6H_2O$ [18, 20]. The proposed structures of single layer of 1.4 nm tobermorite and jennite are shown in Figure 1.3 [18]. The 1.4 nm tobermorite and jennite have a single chain structure with three Si-O tetrahedron units, which is called a dreier single chain. There are two kinds of Si-O tetrahedra, paired (P) and bridging (B). Paired Si-O tetrahedron links to Ca–O layer and no free bonds, while bridging Si-O tetrahedron has two free bonds, which may link to H^+ or Ca^{2+}.

Taylor [17] further proposed that the structure model of C-S-H composed of structurally imperfect 1.4 nm tobermorite and jennite with a defect of dreier single chains of silicate anions. Its schematic model is shown in Figure 1.4. According to this model, the bridging Si-O tetrahedra are sometimes missing, which causes the variation of Ca/Si ratio and finite chain containing 2, 5, 8..., $3n$-1 tetrahedra. This sequence of chain lengths agrees to an existence of a large amount of dimers and pentamers in cement paste cured at room temperature [17, 18]. Unfortunately, the crystal structure of jennite is unknown and many details of the model remained unclear.

1.5 Solid-State NMR of Calcium Silicate Hydrates

Nuclear magnetic resonance (NMR) is sensitive to the local environment around the nuclei and shows the chemical shift due to difference in nature of the chemical bonds, which are so much interesting to the chemists [23]. The NMR for liquids has been utilized for more than 40 years by chemists to identify chemical compounds and now one of the most powerful analytical methods in the chemistry [24]. However the NMR of solid shows a very broad signal (wideline NMR) mainly due to a strong magnetic dipolar interaction [25, 26], which is averaged and cancelled by rapid molecular motion in the liquid. Therefore the information from the solid-state NMR was limited and not interesting for most chemist.

Around 20 years ago, new methodological technologies were developed to obtain high resolution NMR in solids [26, 27, 28, 29]. High-power dipolar decoupling (HD) can cancel the heteronuclear dipolar interaction, in particular by the ^{1}H nuclei. Magic angle spinning (MAS) technique, spinning solid sample along the direction inclined by the magic angle, 54.74°, against the magnetic field direction, can average the chemical shift anisotropy. High-power dipolar decoupling with a magic angle spinning (HD-MAS) technique has become available for chemists by commercially produced solid-state NMR apparatus. The cross polarization (CP) technique is to obtain high sensitive signals of rare spin nuclei such as ^{13}C and ^{29}Si by transferring strong magnetism of the abundant spins such as ^{1}H to the rare spins. CP efficiency strongly depends on the distance between the rare spins and the abundant spins. Therefore, the cross polarization with a magic angle spinning (CP-MAS) technique is used to estimate the existence of ^{1}H near the rare spins.

The solid-state NMR is a powerful technique to study the structure of materials lacking a long-range order such as C-S-H. Useful nucleus for C-S-H are ^{29}Si and ^{1}H.

Lippmaa et al. first applied ^{29}Si MAS NMR to silicates including xonotlite in 1980 [30]. They clarified the chemical shifts ranges of the Q^0, Q^1, Q^2, Q^3 and Q^4 of Si-O tetrahedron units; Q^0: monomeric, Q^1 : end group of silicate chains, Q^2 : middle group of silicate chains or cycles, Q^3 : chain branching site, Q^4 : three-dimensionally cross-linked group [30, 31, 32]. Figure 1.5 shows the notation for building units and silicate anions [32]. Figure 1.6 shows the ranges of chemical shifts of Q^n units of solid silicates [31].

As shown in Figure 1.7, they [30] observed the ^{29}Si MAS NMR signals of synthetic xonotlite. They reported the two signals at –86.8 ppm (Q^2) and –97.8 ppm (Q^3) with a 2:1 intensity ratio [30], which reflect well the double chain structure of xonotlite with a 2:1 ratio of the contents of Q^2 and Q^3 groups.

They applied this method to the cement science [33, 34, 35]. Lippmaa et al. [33] observed ^{29}Si MAS NMR signals of hydration products of tricalciumsilicate (Ca_3SiO_5: C_3S), which is a main component of Portland cement. Two signals were observed at –79 ppm in the end group (Q^1) rang and at –85 ppm in the middle group (Q^2) range. The Q^2 unit signal increased with an increase of reaction time. The silicate chain length of C-S-H was first observed directly and semi-quantitatively. Wieker et al. [34] observed the NMR signals of synthetic 1.4 nm, 1.1 nm and 0.9 nm tobermorites. The NMR spectra of 1.4 nm tobermorite showed a Q^2 signal at –85.3 ppm and a small Q^1 signal at –79.7 ppm, while those of most of 1.1 nm and 0.9 nm tobermorites show Q^3 at –97 ppm in addition to Q^2 and Q^1 signals. They clarified that 1.4 nm tobermorite consists predominantly of single chains and that 1.1 nm and 0.9 nm tobermorites contain double chains and/or single chains depending on the preparation method. Stande et al. [35] observed ^{29}Si HD-MAS and CP-MAS NMR of C-S-H, which were synthesized at 80 °C and 150 °C with starting Ca/Si ratio from 1.0 to 2.0. They discussed about contents of OH groups linked to Si-O tetrahedra of C-S-H. Thereafter many NMR studies of the cement hydration and the structure of the calcium silicate hydrates have been reported [36-48].

Grutzeck et al. [36], Okada et al. [44], Brough et al. [40], and Cong et al. [45, 47] applied the ^{29}Si MAS NMR to study the C-S-H structure. Grutzeck et al. [36] analyzed the C-S-H synthesized at room temperature from fumed silica and lime and concluded that the two structurally distinct C-S-H phases exist. C-S-H with Ca/Si = 0.65 and 1.0 consists predominantly of long silicate anion chains similar to those found in 1.4 nm tobermorite, while C-S-H with Ca/Si =1.1 to 1.3 consists of a mixture of dimer and short chains similar to that reported for synthetic jennite. Okada et al. analyzed the C-S-H hydrothermally synthesized with a starting Ca/Si between 0.3 and 2.0 and evaluated the Q^1 and Q^2 intensities quantitatively. C-S-H contained single silicate anion chains, which became progressively longer as Ca/Si ratio decreased. Brough et al. [40] used the hydration mixture of isotropically enriched amorphous SiO_2 and C_3S

(tricalcium silicate) at room temperature and observed an additional signal at –84 ppm, which was assigned to bridging Q^2. Cong et al. [47] analyzed the room-temperature hydrated C-S-H with Ca/Si of 0.6 – 1.6 and proposed the defect-tobermorite model as a structure model of C-S-H, in which individual layers have the basic structure of 1.4 nm tobermorite but contain a significant concentration of defects and are more distorted. They [45] concluded that C-S-H with Ca/Si > 1.0 have many dimers and relatively long chains in the structure according to the analysis of CP-MAS spectra.

The formation process of xonotlite has not been studied by ^{29}Si MAS NMR yet but that of tobermorite has been reported by Mitsuda et al. [41], Sato et al. [38] and Okada et al. [43]. Tobermorite is hydrothermally synthesized from silica and lime mixture in the same manner as xonotlite. The Ca/Si ratio of tobermorite is 0.83 lower than that of xonotlite, 1.0, and the ordinary hydrothermal temperature for tobermorite is about 180 °C lower than that for xonotlite, about 200 °C.

Mitsuda et al. [41] first applied ^{29}Si MAS NMR for the formation process of tobermorite. When quartz was used as starting siliceous material, Ca-rich C-S-H with Ca/Si ratio above 1.0 was formed initially, then the C-S-H changed to tobermorite. When amorphous silica was used, C-S-H with Ca/Si ratio of 0.8 was formed rapidly then this C-S-H was stable and very slowly converts to tobermorite. They confirmed that 1.1 nm tobermorite consists of double chain silicate anions. They observed the Q^2/Q^3 ratio decreased with reaction time.

Sato et al. [38] paid attention to the structure of C-S-H initially formed from different siliceous materials, quartz and amorphous silica. They clarified that the structure of the C-S-H formed from quartz was different from that of the C-S-H formed from amorphous silica. The C-S-H form quartz showed a low Q^2/Q^1 intensity ratio, which suggested that the C-S-H contained short silicate chains and dimers. The C-S-H formed from amorphous silica had a high Q^2/Q^1 intensity ratio and a Q^3 peak, which indicates the presence of long and cross-linked silicate chains. They concluded that the C-S-H from amorphous silica was harder to crystallize to tobermorite due to the presence of a long and cross-linked silicate chains and that the C-S-H from quartz easily crystallized due to its short silicate chain structure. They observed the three Q^2 signals at –82 ppm, –85 ppm, and –92 ppm on the process of tobermorite formation and finally the signals at –82 ppm and –92 ppm disappeared. The signal at –82 ppm was assigned

to bridging tetrahedra that have not yet bonded to other bridging tetrahedra. The signal at –85 ppm was assigned to paired tetrahedra. The signal at –92 ppm was assigned to bridging tetrahedra that are connected by hydrogen bond. Okada et al. [43] studied the similar system by ^{29}Si NMR and analytical TEM, and obtained the same conclusion that C-S-H with higher than Ca/Si of 0.99 easily changed to tobermorite and that the C-S-H from amorphous silica has partly cross-linked structure and hardly change to tobermorite.

^{1}H NMR was also applied to the calcium silicate hydrates. Grimmer and Wieker [49] first observed the ^{1}H wideline NMR of synthetic xonotlite and determined the H types in xonotlite by analyzing the line shape. ^{1}H MAS NMR signals of synthetic xonotlite were reported by Rosenberger et al. [50]. Heidemann [51] summarized the application of ^{1}H NMR to cement science. Rassem e al. [52] reported the CRAMPS NMR of C_3S hydration.

1.6 Summary

The formation of xonotlite proceeds from CaO and SiO_2 through intermediate phases, such as C-S-H (poorly crystalline calcium silicate hydrate), α-C_2SH (dicalcium silicate hydrate) and tobermorite. The reaction process heavily depends on the starting siliceous materials. To explain this dependence on the starting siliceous materials, the effects of the differences of the concentration of dissolved silica in the hydrothermal solution and the type of the C-S-H formed were suggested.

The reaction occurs in a suspension, which is composed of the mixture of the starting materials, $Ca(OH)_2$ and silica, intermediate phases and produced xonotlite. Due to the complexity of the reaction system, the reaction mechanics has been still unclear. Particularly the reaction process from C-S-H to xonotlite has not been studied in detail.

In this thesis, I pay attention to the reaction step from poorly-crystalline calcium silicate hydrate (C-S-H) to xonotlite and clarify the crystallization mechanism of xonotlite using solid-state NMR as follows. This is the first application of NMR to the xonotlite formation process.

1) To study the variation of C-S-H structure with Ca/Si ratio, the Ca/Si ratio of C-S-H is changed by two methods. One is to vary the Ca/Si ratio of the starting materials. The other is H-type ion exchange resin treatment of C-S-H with a high Ca/Si ratio. The structural change of C-S-H is analyzed by NMR and discussed.

2) The formation of xonotlite is separated into two reaction steps, C-S-H formation and xonotlite formation. The formation step of xonotlite from C-S-H is targeted and investigated by TEM observation, the degree of formation (α) evaluated by thermogravimetry, and ^{29}Si solid-state NMR spectroscopy. Using this step-by-step method, the reaction system is simplified and its microstructural change is discussed more directly.

3) The reaction process of formation of xonotlite heavily depends on the starting siliceous material. The structure of the C-S-H formed in the early stage might vary according to the starting siliceous materials and that the structure of C-S-H affects the stability of C-S-H and determine the next reaction step. The structure of the C-S-H in the reaction process of xonotlite formation using the 4 kinds of siliceous materials is analyzed by ^{29}Si NMR and XRD. The influence of siliceous materials on the crystallization of xonotlite is examined.

4) I observed the high-resolution ^{29}Si and ^{1}H MAS NMR spectra of the natural xonotlite and the synthetic xonotlite with high crystallinity. The xonotlite crystal structure is examined by the NMR signals in detail.

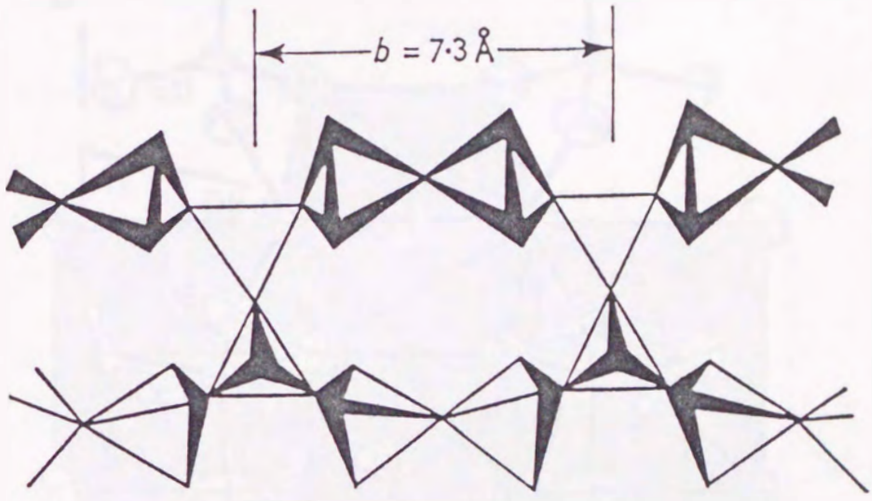

Figure 1.1 Dreier double chain of silicate anions of xonotlite from Mamedov and Belov [7].

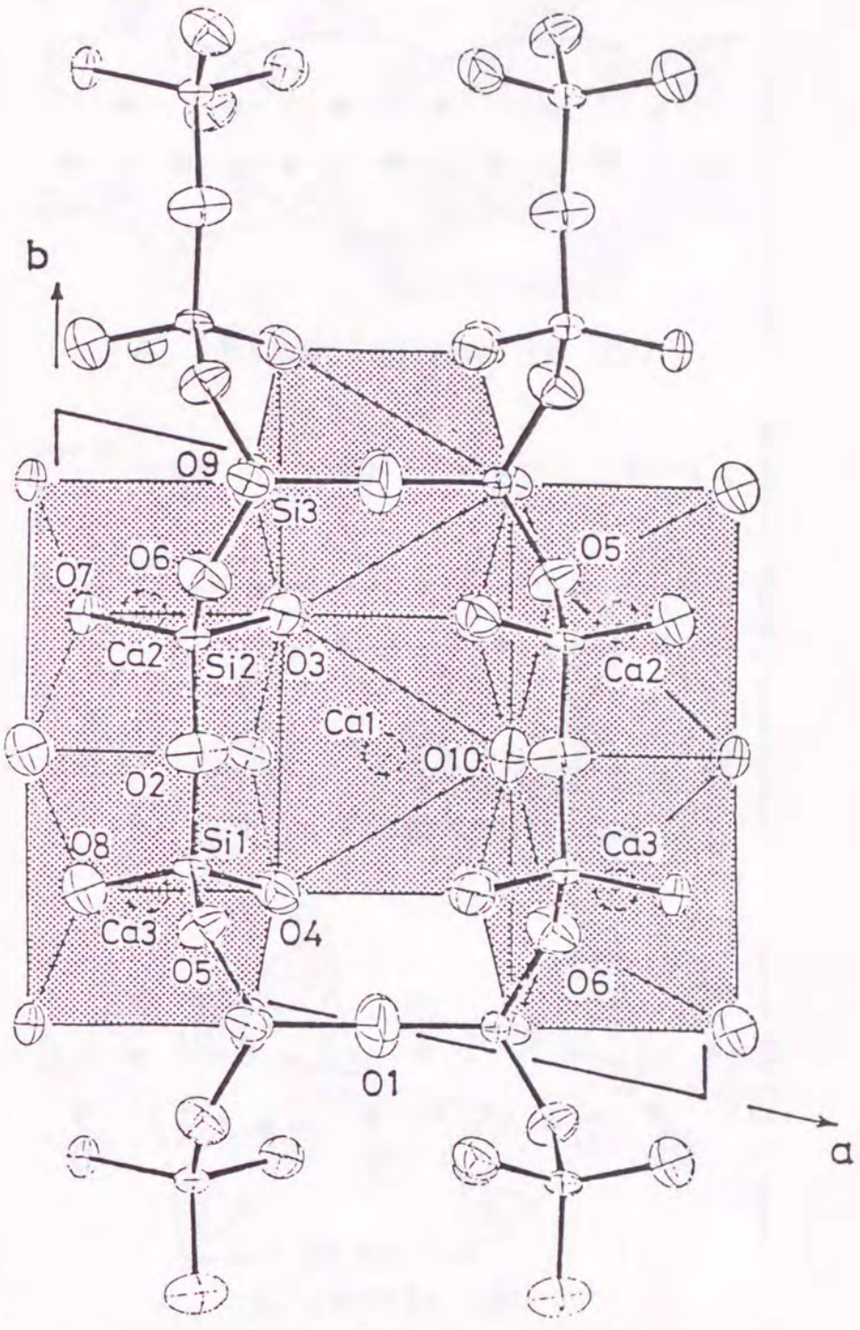

Figure 1.2 The projection of xonotlite structure determined by Kudoh and Takéuchi [10]. The Si–O bonds are shown by heavy lines.

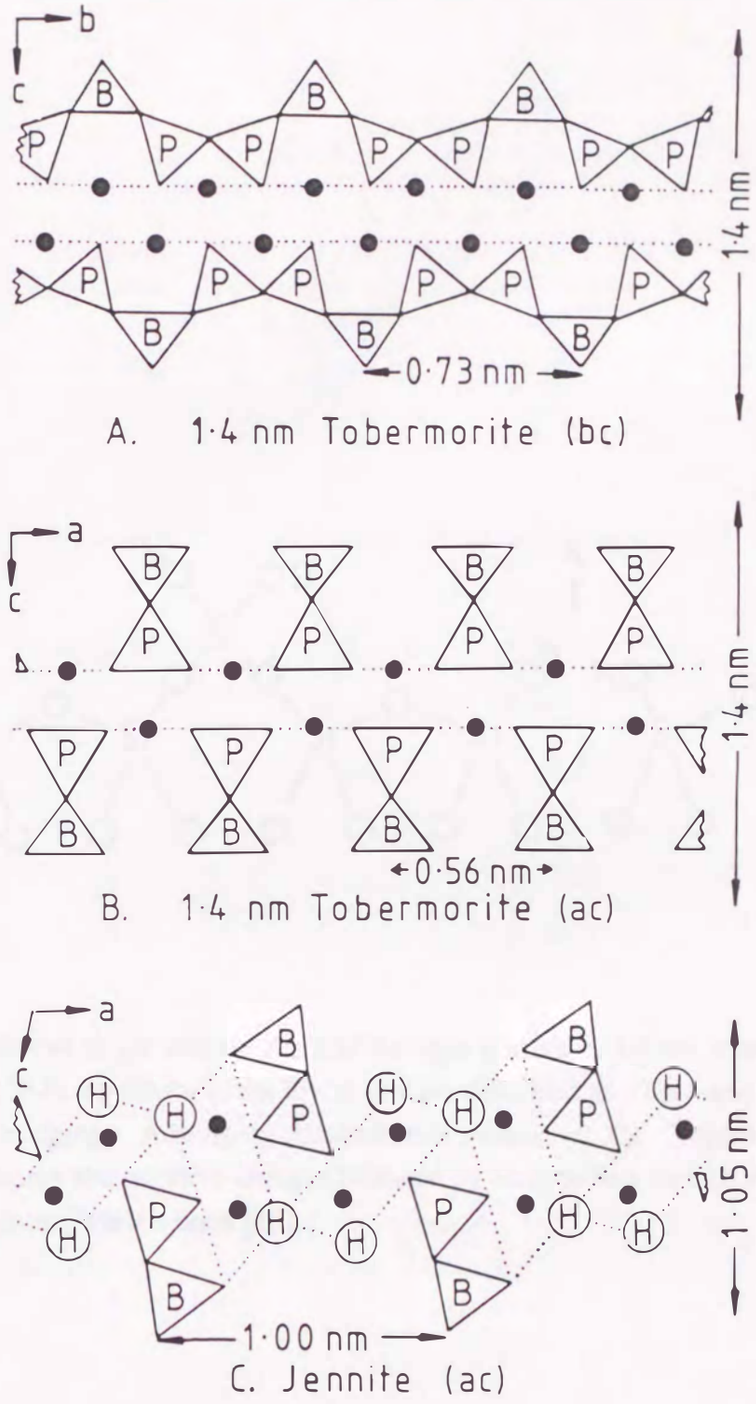

Figure 1.3 (A) and (B) Structure of a single layer of 1.4nm tobermorite in *bc*- and *ac*-projection, respectively. (C) Suggested structure for a single layer of jennite in *ac*-projection. Full circles and 'H's denote calcium atoms and hydroxyl groups, respectively. P and B denote pared and bridging tetrahedra, respectively. These figures are from Taylor's book [18].

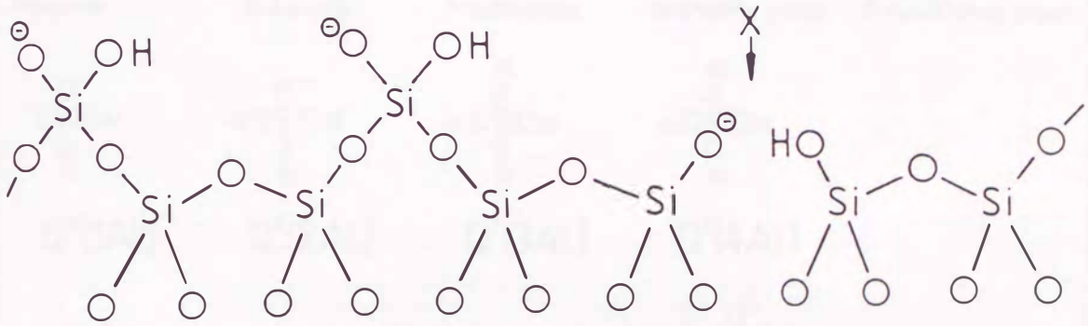

Figure 1.4 Dreier single silicate chain of the type present in 1.4 nm tobermorite and jennite. The Si-O tetrahedra in the lower row are described as paired and those in the upper row as bridging. A bridging tetrahedron is missing (at X). Suggested position of hydrogen atoms and negative charges balanced by intermediate cations are included. This figure is from Taylor's book [18].

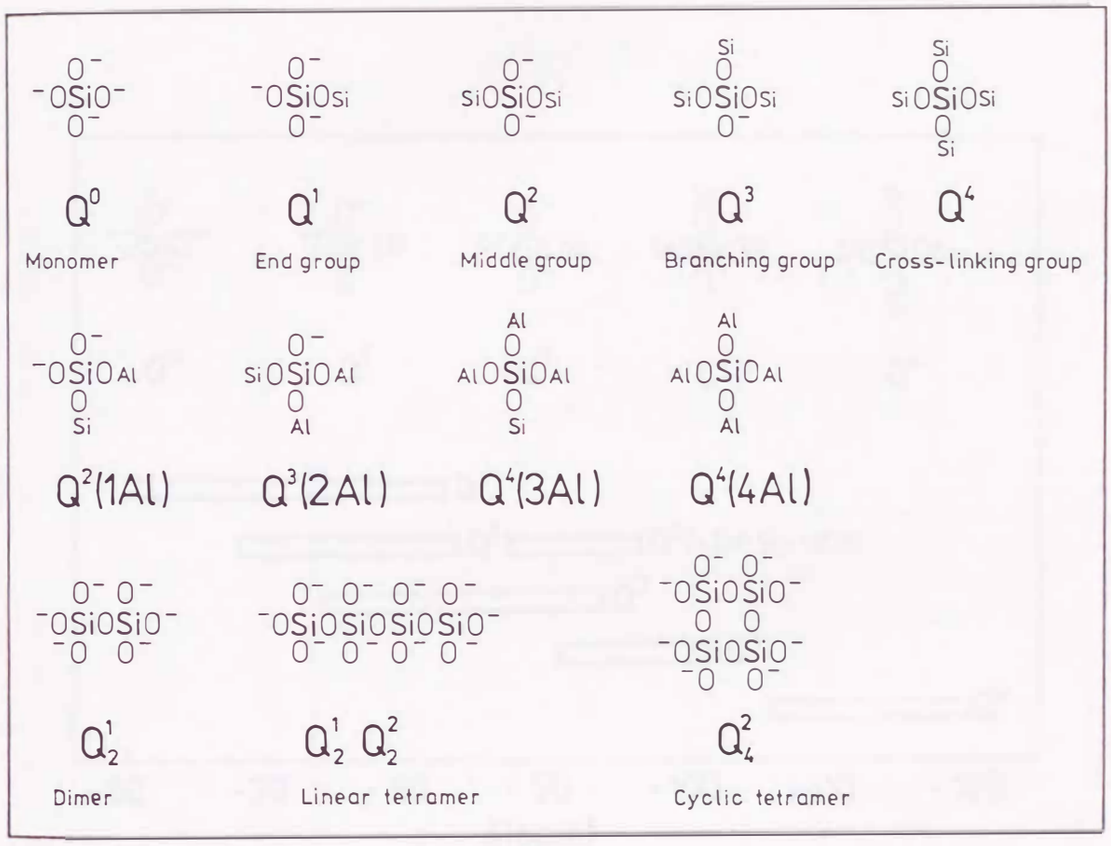

Figure 1.5 Notation for building units and silicate anions. Top, Q^n units of silicate; center, examples of $Q^n(m\mathrm{Al})$ units of aluminosilicates; bottom, examples of silicate anions [32].

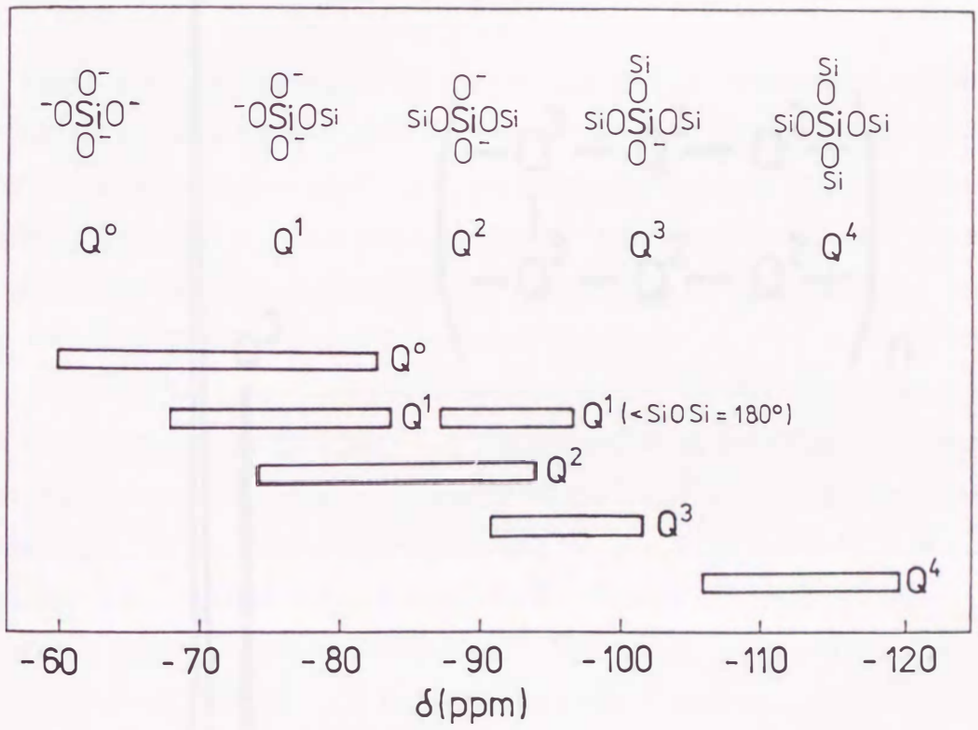

Figure 1.6 Ranges of ^{29}Si chemical shifts of Q^n units in solid silicates [31].

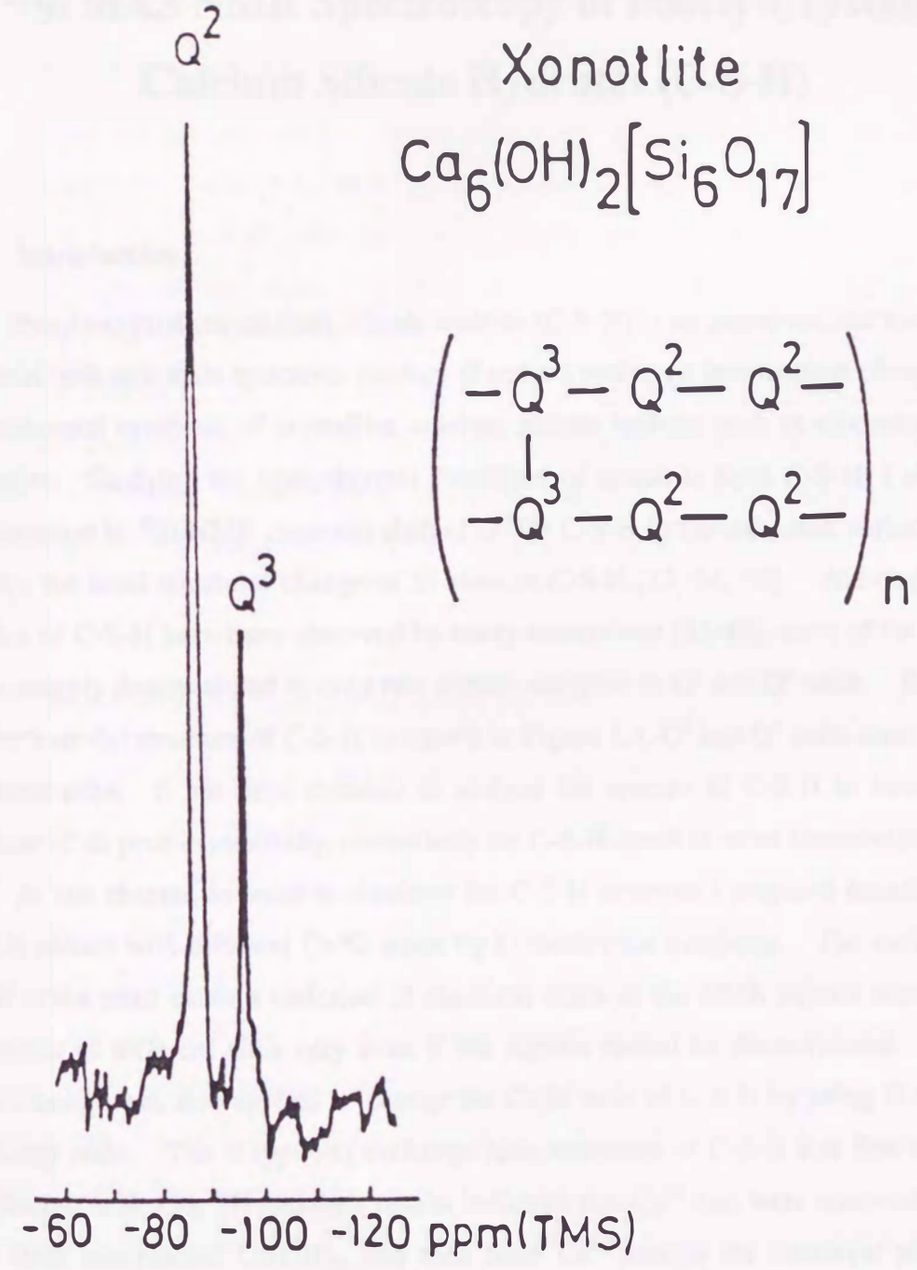

Figure 1.7 ^{29}Si MAS NMR signals of synthetic xonotlite [30].

Chapter 2

^{29}Si MAS NMR Spectroscopy of Poorly-Crystalline Calcium Silicate Hydrates (C-S-H)

2.1 Introduction

Poorly-crystalline calcium silicate hydrate (C-S-H) is an important and interesting material both as a main hydration product of cement and as an intermediate phase on the hydrothermal synthesis of crystalline calcium silicate hydrate such as tobermorite and xonotlite. Studying the hydrothermal formation of xonotlite from C-S-H, I observed the variation in ^{29}Si NMR chemical shift of Q^2 for C-S-H in the induction period, which reflects the local structural change of Si atom in C-S-H [53, 54, 55]. Although NMR spectra of C-S-H have been observed by many researchers [33-48], most of the spectra were roughly deconvoluted to only two signals assigned to Q^1 and Q^2 units. Based on Taylor's model structure of C-S-H as shown in Figure 1.4, Q^1 and Q^2 units must contain different sites. It has been difficult to analyze the spectra of C-S-H in more detail because of its poor-crystallinity, particularly for C-S-H cured at room temperature.

In this chapter, in order to elucidate the C-S-H structure I prepared homogeneous C-S-H phases with different Ca/Si ratios by hydrothermal synthesis. The variation of Ca/Si ratios must cause a variation of chemical shifts of the NMR signals because the quantities of different sites vary even if the signals cannot be deconvoluted. H-type ion exchange was also applied to change the Ca/Si ratio of C-S-H by using H-type ion exchange resin. The H-type ion exchange resin treatment of C-S-H was first analyzed by Nishino et al. [56, 57] and their results indicated that Ca^{2+} ions were removed step by step from non-reacted $Ca(OH)_2$, and then from Ca^{2+} ions in the interlayer sites, and finally from Ca–O polyhedra. Using this ion exchange treatment, I expected to remove Ca^{2+} ions in the interlayer site of C-S-H without destruction of Si–O tetrahedra

and Ca–O polyhedra, which affects the chemical shifts of Q^1 and Q^2 without change of their quantities.

2.2 Experimental

2.2.1 Preparation of C-S-H

C-S-H was hydrothermally synthesized at 130°C for 2 hr from CaO and silica with Ca/Si molar ratios between 0.6 and 2.0 in a stirred suspension of a water/solid weight ratio of 40. CaO was obtained by heating reagent grade $CaCO_3$ at 1000°C for 4 hr. The used silica was amorphous and its ignition loss was 50%. First, CaO was added into 1/6 of total water and the suspension was vigorously stirred by a ultradisperser for 2 min. Then silica and the remaining water were added and the suspension was stirred again before autoclaving. Using this method, I obtained a homogeneous C-S-H with a spread thin foil-like morphology as shown in Figure 3.2 [53]. The products were filtered and dried in vacuum at 60°C for 2 days and then characterized by XRD and NMR.

2.2.2 Treatment by H-Type Ion Exchange Resin

Two types of H-type ion exchange resin (H-R) were used. One (H-R A) was a strong acid type containing a sulfonic group (SO_3H) [MCI GEL CK08P from Mitsubishi Chemical Corp.]. The other (H-R B) was a weak acid type containing a meta-acrylic group ($-CH_2-C(CH_3)COOH-$), [DIAION WK100 from Mitsubishi Chemical Corp.]. The size distribution of H-R A was between 75 and 150 μm, while that of H-R B was between 300 and 1200 μm. Each H-R was washed well with distilled water until the washing water showed no color and dried in vacuum at 60°C for 2 days. A total ion exchange capacity of H-R A was 4.6 meq/g [57] and that of H-R B is estimated to be about 4.2 meq/g in the catalogue.

A suitable amount of H-R was added into 50 ml distilled water. After 10 min, 1 g of C-S-H with a starting Ca/Si ratio of 1.5 was added into the suspension and stirred for different periods at ambient temperature. The samples were filtered and dried in vacuum at 60°C for 2 days. H-R A was separated from the sample through 45 μm

sieve after drying. H-R B was separated from the sample through 297 μm sieve at the filtration. The quantities of H-R and the treatment time were varied.

The C-S-H with a starting Ca/Si of 1.5 contained 10 mmol Ca ions per 1 g, which was calculated from the ignition loss, 22.5%, at 1000 °C of the C-S-H. The quantities of H-R to exchange Ca ions from 1 g of C-S-H completely were estimated to be 4.5g of H-R A and 5.0 g of H-R B, respectively, from their ion exchange capacities.

2.2.3 ^{29}Si NMR and XRD Measurements

^{29}Si NMR spectra were recorded on a Bruker DSX300WB (7.05 T magnetic field) at 59.6 MHz by use of high power decoupling (HD) or cross polarization (CP) with magic angle spinning (MAS) of 5 kHz. HD-MAS spectra were acquired with a repetition time of 40 s, the use of $\pi/4$ pulses (2.5 μs) and an accumulation number of 1024 and plotted with a line broadening factor of 20 Hz. For CP-MAS spectra, the repetition time, the contact time (CT), the accumulation number and the line broadening factor were 5 s, 2 ms, 1024 and 20 Hz, respectively. The chemical shifts were referenced to TMS by use of 3-(trimethylsilyl)-propane sulfonic acid sodium salt (DSS) as a secondary reference (+1.53 ppm). The line-shape of NMR spectra was analyzed using a Bruker line-fitting program, WinFit, with 50% Gaussian and 50% Lorentzian mixture functions.

XRD powder patterns were recorded with Cu $K\alpha$ radiation on Rigaku RAD-II A. A 0.02° 2θ step size and 1-second count time were used.

2.3 Results and Discussion

2.3.1 XRD patterns of C-S-H

The XRD patterns of C-S-H are shown in Figure 2.1. The pattern exhibited relatively sharp reflections at 0.18 nm (2θ =49.7°), 0.28 nm (32.1°), and 0.30 nm (29.3°), which is typical for C-S-H(I) [17]. The XRD results agreed well with those previously observed by Okada et al. [42]. In the XRD pattern of C-S-H with near Ca/Si ratio of 0.8, a broad basal reflection was observed.

Non-reacted $Ca(OH)_2$ was detected for the samples with Ca/Si ≥ 1.5. A broad peak of amorphous silica near 2θ of 23° was not detected for all samples. Because the

concentrations of Ca^{2+} and silicate ions in the reaction solution were negligible [53], therefore the Ca/Si ratio of C-S-H with a starting Ca/Si ratio < 1.5 were nearly equal to the starting one, which was confirmed by chemical analyses in the previous work [56]. According to an evaluation of the quantity of non-reacted $Ca(OH)_2$ from TG loss of the dehydration of $Ca(OH)_2$ near 450 °C [56], the Ca/Si ratio of C-S-H with a starting Ca/Si ratio of 1.5 was estimated to be 1.44. The C-S-H phases with starting Ca/Si ratios ≥ 1.5 were estimated to be a mixture of C-S-H with Ca/Si ~ 1.5 and non-reacted $Ca(OH)_2$.

The spacing of 0.18 nm did not change with composition and the spacing of 0.30 nm increased only by ca. 0.002 nm with a decrease of Ca/Si ratio. This indicates that Ca–O layer structure dose not change drastically with a Ca/Si ratio, because the reflection peaks of C-S-H correspond to the important repeat distance of the Ca–O layer structure [17].

2.3.2 NMR spectra of C-S-H

The ^{29}Si HD-MAS and CP-MAS NMR spectra of C-S-H hydrothermally synthesized are shown in Figure 2.2. The typical deconvoluted lines of the HD-MAS spectra of C-S-H with a starting Ca/Si ratio of 1.8 and 0.8 are shown in Figure 2.3. The chemical shifts and relative intensities are summarized in Table 1.

At least five lines were needed to obtain a good line-fitting. I assigned them to two kinds of Q^1 units (Q^1_H –79 ~ –80 ppm, Q^1_L –81 ppm) and three kinds of Q^2 units (Q^2_H –82.5 ppm, Q^2_M –84 ~ –86 ppm, Q^2_L –91 ppm) as shown in Table 1. Q^1_H between –79 and –80 ppm and Q^2_M between –84 and –86 ppm are typical signals of C-S-H and reported by many researchers [33, 35, 36, 40, 42, 45]. I succeeded in observing additional three signals at –81, –82.5 and –91 ppm. One reason for this is that our C-S-H was hydrothermally synthesized and its crystallinity was relatively higher than ordinary C-S-H cured at room temperature. Another reason is that the Ca/Si ratio of C-S-H was systematically varied from 0.6 to 1.5. The Q^1_L signal at –81 ppm is first reported. The Q^2_H signal at –82.5 ppm was observed and assigned to Q^2 unit by Brough [40] and Sato [38], while Okada assigned it to Q^1 unit [42]. The broad signal Q^2_L at –91 ppm was observed for 1.1 nm tobermorite formation process and assigned to Q^2 by Sato [38] and

Okada [42]. Its structure is not still clear but tentatively I also assigned this signal to Q^2 unit.

The NMR spectra of C-S-H phases with starting Ca/Si ratios ≥ 1.2 show almost the same tendency, which supports that the real Ca/Si ratio of C-S-H with a starting Ca/Si ratio ≥ 1.5 is the same, as previously mentioned in 2.3.1. The Q^1_H signal at –79.1 (45%) and the Q^2_M signal at –84.3 ppm (50%) are the main signals and about 3-6% of Q^1_L signal appeared. C-S-H with Ca/Si ratio ≤ 1.0 has Q^1_H, Q^2_H, Q^2_M and Q^2_L signals and their chemical shifts and relative intensities vary with Ca/Si ratios. With a decrease of Ca/Si ratio, the intensities of the Q^1_H signal decreased from 48 to 10%, while the total intensities of signals of Q^2 units increased, which indicates an increase of the mean chain length of silicate anion. The chemical shifts of Q^2_M signal showed a lower frequency shift from –84.2 to –85.6 ppm. The signals Q^1_H, Q^2_H and Q^2_L were enhanced by CP-MAS.

2.3.3 Ion Exchange Resin Treatment

^{29}Si HD-MAS and CP-MAS NMR spectra of C-S-H treated by strong acidic H-type ion exchange resin (H-R A) are shown in Figure 2.4. The treatment time was 2 hr and the quantities of H-R A added were 0, 1, 2, 3 g.

In Figure 2.4 (a), the Q^1 signal decreases and the Q^2 signal becomes sharper with a lower-frequency chemical shift by treatment with a larger amount of H-R A. By addition of 3 g of H-R A, the signal Q^2_H at –82.5 ppm, which is a typical signal of C-S-H with a lower Ca/Si ratio than 0.8 as mentioned above, and a broad signal from –90 to –110 ppm appear. A part of the broad signal from –90 to –110 ppm may be due to silica gel (Q^3 : ~ –102 ppm, Q^4 : ~ –112 ppm).

The spectra of C-S-H with a starting Ca/Si ratio of 1.5 seems to change to those of C-S-H with lower Ca/Si ratios. The Ca/Si ratios of C-S-H treated by H-R A have not been analyzed yet. But these Ca/Si ratios can be estimated from the ion exchange capacity, 4.6 meq/g, of H-R A. The Ca/Si ratios of C-S-H treated by H-R A are estimated to be 1.17 for addition of 1 g of H-R A, 0.83 for 2 g, 0.5 for 3 g, respectively. When the spectra of C-S-H with the same Ca/Si ratios are compared, the HD-MAS and CP-MAS spectra in the Figure 2.2 agree well with those in Figure 2.4. It is concluded

that Ca^{2+} ions of C-S-H with Ca/Si of 1.5 were leached and C-S-H with lower Ca/Si was formed by this H-R treatment.

Using the ion exchange treatment, I expected to remove Ca^{2+} ions in the interlayer site of C-S-H without destruction of Si–O tetrahedra and Ca–O polyhedra structures, which affects the chemical shift of Q^1 and Q^2 without change in their quantities. But the same C-S-H with a lower Ca/Si ratio was obtained. Considering the hydration time of C-S-H cured at room temperature, I thought the treatment of 2 hr was not enough for the rearrangement of Si–O tetrahedra and Ca–O polyhedra structure. To examine the process of H-R treatment in detail, the treatment time was varied and a weak acid type resin (H-R B) was also applied.

The ^{29}Si HD-MAS NMR spectra of C-S-H treated for various treatment time by 3 g of H-R A and 6 g of H-R B are shown in Figure 2.5. The treatment time was varied from 2 min to 20 min.

In Figure 2.5 (a), the signals abruptly change at only 2 min of treatment time of H-R A. The Q^1 signal abruptly decrease. The Q^2 signal become sharp and its chemical shift shows a lower-frequency shift from –84.3 ppm to –85.5ppm. A broad signals near –100 and –110 ppm, which are assigned to Q^3 and Q^4 of silica gel respectively, appear. By longer than 5 min treatment, the broad signals near –100 and –110 ppm decrease, Q^1 decreases and Q^2 becomes sharper. In Figure 2.5 (b), the variation of Q^1 and Q^2 signals of C-S-H treated by H-R B shows the similar tendency but is much slower compared with H-R A. By a longer treatment of H-R B, Q^1 signal decreases and Q^2 signal becomes sharper with lower-frequency shift. The broad signals near –100 and –110 ppm due to silica gel appears only after 10 min and their intensities are much smaller than those of H-R A.

It is found out that the decrease of Q^1 signals occurred rapidly (2 min) for both H-R A and H-R B treatment. By the H-R A treatment, a large amount of silica gel was formed at the same time. Therefore, the destruction of C-S-H silicate structure also occurred. On the other hand, by the H-R B treatment silica gel was formed after 10 min and its quantity was very small. Therefore the treatment of H-R B is considered to remove preferably the Ca^{2+} ions in the interlayer sites without destruction of C-S-H structure at least in the early stage.

2.3.4 Structure Model of C-S-H

The structure model of C-S-H with a defect of single dreier chain of silicate anions was proposed by Taylor [17] and its schematic model was shown in Figure 2.6 (a). According to this model, there are two types of Q^2 units, paired (P) and bridging (B). Paired Q^2 links to Ca–O layer and has no free bonds, while bridging Q^2 has two free bonds, which may link to H^+ or Ca^{2+}. The bridging Q^2 are sometimes missing, which causes the variation of Ca/Si ratio and finite chain containing 2, 5, 8..., $3n$-1 tetrahedra. This sequence of chain lengths agrees to an existence of a large amount of dimers and pentamers in cement paste cured at room temperature [17].

The variety of Q^2 in this model can explain the variation of the chemical shifts of Q^2 units. The signal at –85.6 ppm for C-S-H with Ca/Si ratio ≤ 0.8 can be assigned to paired Q^2 because the chemical shift agrees well with that of 1.1 nm tobermorite containing only paired Q^2 [34]. The chemical shift of bridging Q^2 bound by Ca^{2+} is considered to be near –84 ppm because C-S-H with Ca/Si ratio ≥ 1.5 must have only bridging Q^2 with Ca^{2+} and paired Q^2. With a decrease of Ca/Si, the amount of bridging Q^2 bound by H^+ increases and the chemical shift of bridging Q^2 must be different from that of paired Q^2. According to Janes and Oldfield [58], a signal of ^{29}Si NMR shifts toward higher frequency by 0.43 ppm when Si–OCa changes to Si–OH. Therefore the signal Q^2_H at –82.5 ppm can be assigned to bridging Q^2 bound by H^+. The enhancement of this signal by CP also supports this assignment. The intensity of Q^2_H signal was nearly a half of that of Q^2_M signal for C-S-H with Ca/Si ratio ≤ 0.7, which corresponds well to the ratio 1:2 of bridging Q^2 units to paired ones. The structure due to the broad signal Q^2_L at –91 ppm is not clear though Sato et al. assigned –91 ppm signal to bridging Q^2 units connected each other by hydrogen bonds [38]. With a decrease of Ca/Si ratio the intensity of Q^1 units decreased, which can be explained by the decrease of defects of silicate anions. The mean chain length increased with a decrease of Ca/Si ratio.

H-R treatment results indicate that the removal of Ca^{2+} ions from C-S-H causes an abrupt decrease of Q^1 units in a very short time (2 min). A strong acid type H-R A partially destroyed the structure of C-S-H but a weak acid type H-R B did not damage the structure. According to Taylor's model, silicate chains are separated by defect of bridging Q^2 as shown in Figure 2.6 (a). Although Ca^{2+} ions are removed from bridging

Q^2 or Q^1, it does not automatically cause the decrease of Q^1 on this model. The Si–O tetrahedra linking to the Ca–O polyhedra destroyed by the attack of H^+ may move to the defects of bridging Q^2 and connect the silicate chains. This mechanism may occur but the treatment time was too short compared with hydration time of cement cured at room temperature. I have to consider the structure that automatically increases the silicate chain length by removing Ca^{2+}. If silicate chains were separated by insertion of Ca^{2+} ions between Si–O tetrahedra as shown in Figure 2.6 (b), the removal of Ca^{2+} ions will increase the silicate chain length. The separation of silicate chain by insert of Ca^{2+} can occur only when there are a large amount of Ca^{2+} ions in the interlayer sites. The Q^1_L signal at –81 ppm, which appeared only for C-S-H with a Ca/Si ratio ≥ 1.2, may be assigned to Q^1 units separated by Ca^{2+} ions though its intensity was smaller than expected. Q^1_H signal at –79 ppm is assigned to paired Q^1 caused by the defects of bridging Q^2.

2.4 Conclusions

C-S-H phases were prepared hydrothermally at 130°C for 2 hr with Ca/Si ratios between 0.6 and 2.0. H-type ion exchange was also applied to change the Ca/Si ratio of C-S-H by using H-type ion exchange resin. The structural change of C-S-H with Ca/Si molar ratio was studied by ^{29}Si NMR.

1) The NMR spectra of hydrothermally synthesized C-S-H were deconvoluted to 5 signals, which were assigned to two kinds of Q^1 units (Q^1_H –79 ~ –80 ppm, Q^1_L – 81 ppm) and three kinds of Q^2 units (Q^2_H –82.5 ppm, Q^2_M –84 ~ –86 ppm, Q^2_L –91 ppm). With a decrease of Ca/Si ratio, the intensity of Q^1 unit signals decreased, the position of Q^2_M signal shifted from –84.2 ppm to –85.6 ppm. Q^2_H at –82.5 ppm appeared for C-S-H with Ca/Si ≤ 1.0. The Q^1_H, Q^2_H and Q^2_L signals were enhanced by CP.
2) The signals were assigned on the basis of Taylor's structure model. The Q^2_M signal at –85.6 ppm and the Q^2_H signal at –82.5 ppm are assigned to the paired Q^2 and the bridging Q^2 with OH, respectively. Bridging Q^2 bound by Ca^{2+} ions is considered to be near –84 ppm.

3) The C-S-H phase with Ca/Si of 1.5 was treated by H-type ion exchange resin at room temperature. Ca^{2+} ions of C-S-H with Ca/Si of 1.5 were leached and C-S-H with lower Ca/Si was formed. It was found out that the Q^1 units decrease rapidly (2 min) by this treatment. To explain this abrupt decrease of Q^1, the separation model of silicate anions by insertion of Ca^{2+} ions was proposed. The Q^1_L signal at –81 ppm was assigned to Q^1 units separated by Ca^{2+} ions.

Table 2.1 Chemical shifts (δ) and relative intensities (*I*) of ^{29}Si HD-MAS NMR signals of C-S-H synthesized hydrothermally at 130°C.

Initial Ca/Si	Q^1_H		Q^1_L		Q^2_H		Q^2_M		Q^2_L	
	δ (ppm)	*I* (%)	δ (ppm)	*I* (%)	δ (ppm)	*I* (%)	δ (ppm)	*I* (%)	δ (ppm)	*I* (%)
2.0	−79.0	47.4	−81.0	4.4			−84.2	48.3		
1.8	−79.1	43.2	−81.3	5.5			−84.4	51.3		
1.5	−79.2	48.0	−81.0	3.4			−84.3	48.6		
1.2	−79.1	39.2	−81.6	3.3			−84.3	57.5		
1.0	−79.3	26.1			−82.3	10.7	−84.8	63.2		
0.8	−79.7	15.5			−82.9	18.1	−85.4	53.5	−90.9	12.9
0.7	−79.9	10.7			−83.0	23.5	−85.6	52.6	−90.6	13.3
0.65	−79.7	10.3			−83.1	22.9	−85.6	52.8	−91.4	14.0
0.6	−79.4	10.8			−82.4	22.2	−85.5	49.1	−92.1	17.9

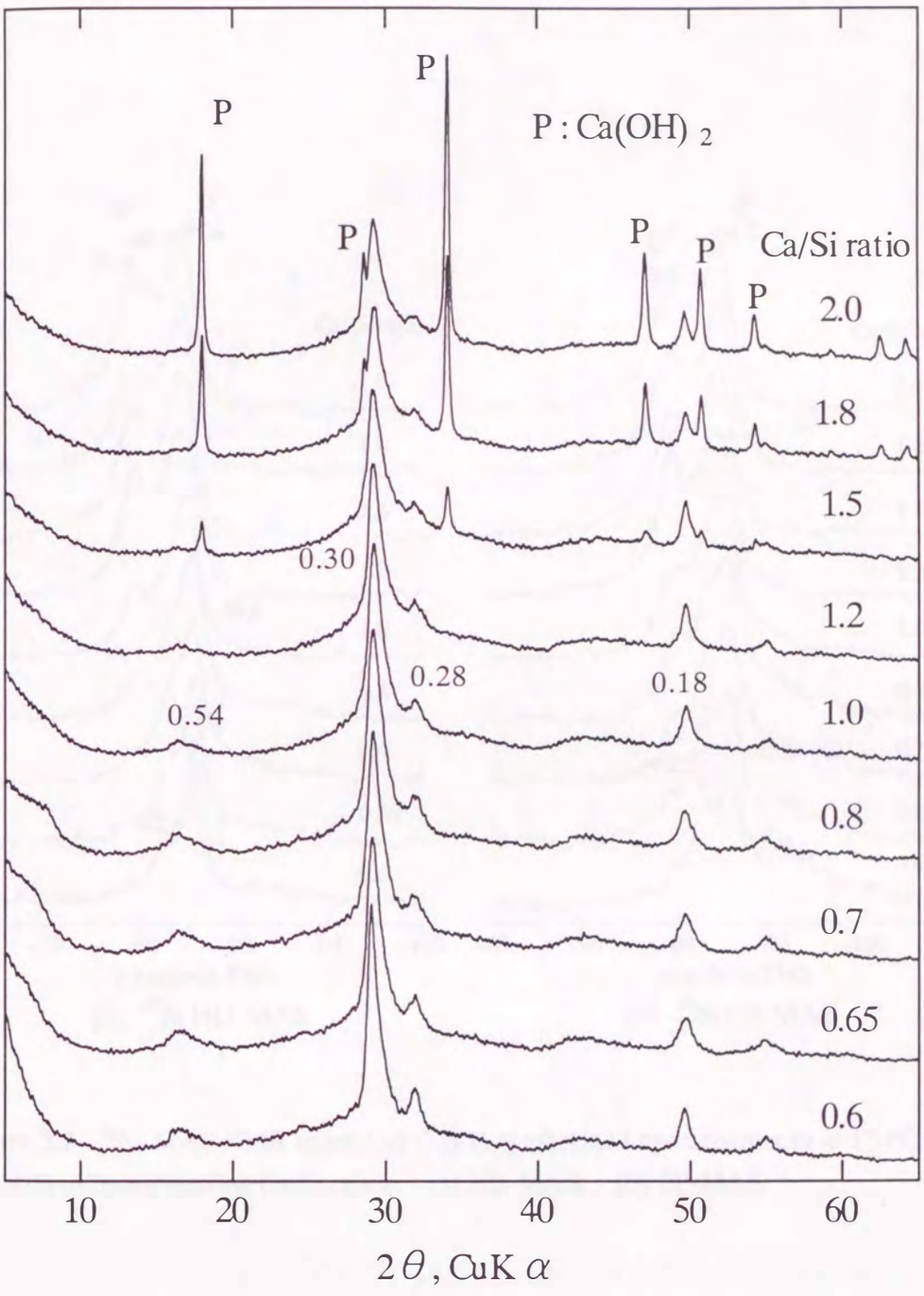

Figure 2.1 XRD patterns of C-S-H synthesized hydrothermally at 130°C for 2 hr with different starting Ca/Si ratios.

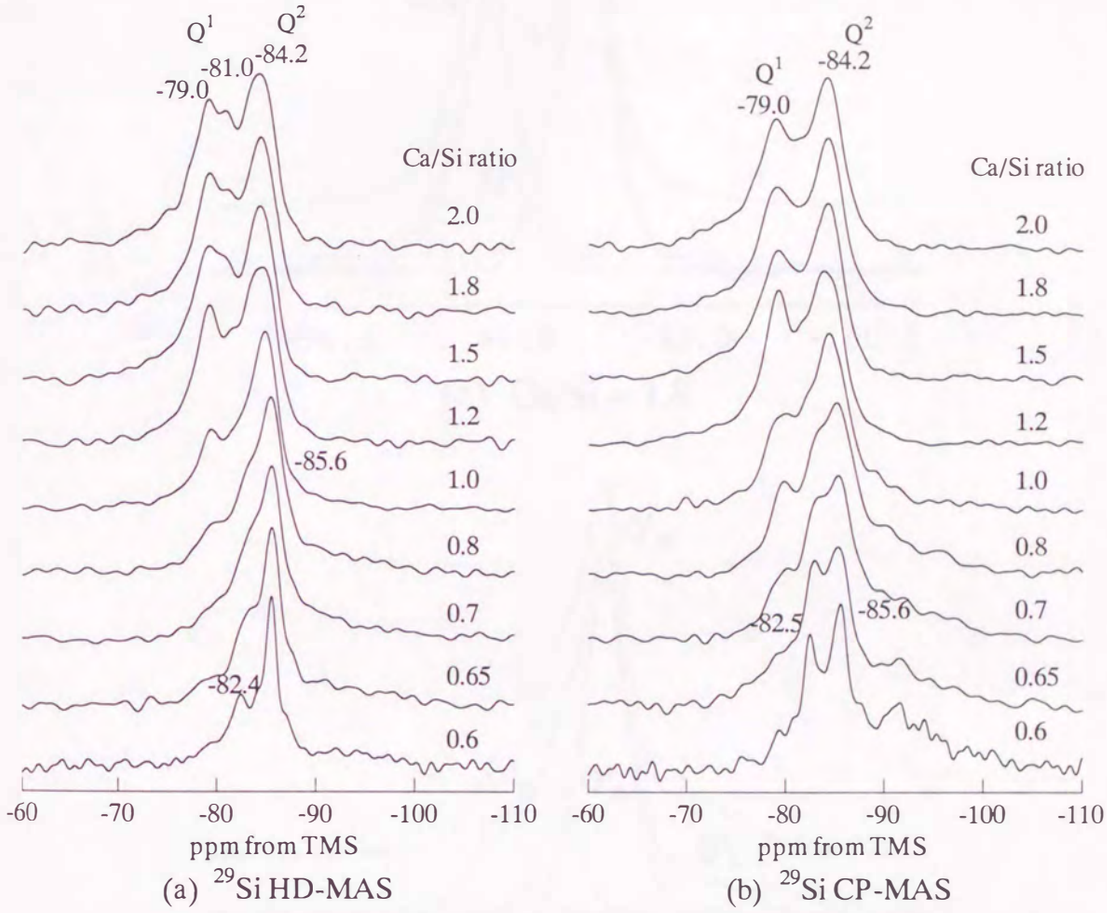

Figure 2.2 ^{29}Si MAS NMR spectra of C-S-H synthesized hydrothermally at 130°C for 2 hr with different starting Ca/Si ratios. (a) HD-MAS, (b) CP-MAS.

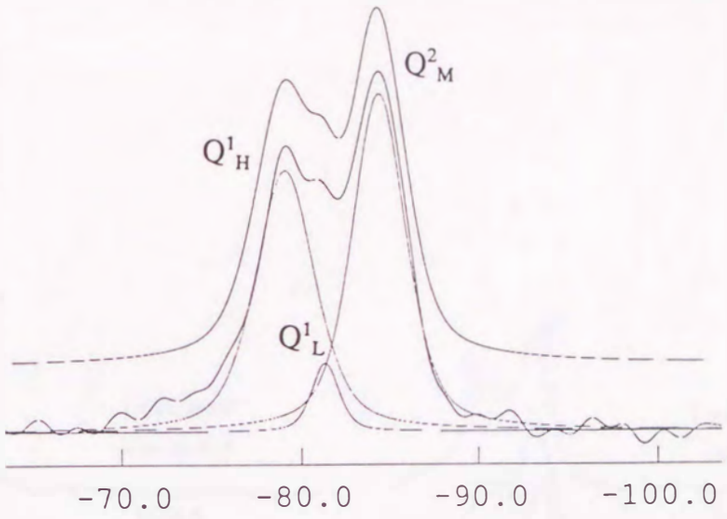

(a) Ca/Si = 1.8

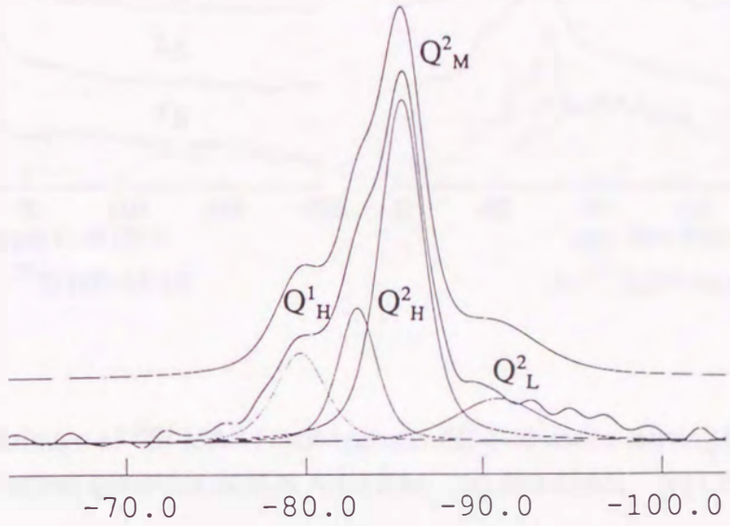

(b) Ca/Si = 0.8

Figure 2.3 Line-fitting of ^{29}Si HD-MAS NMR spectra of C-S-H synthesized hydrothermally at 130°C for 2 hr. Upper lines are simulation lines.
(a) Ca/Si=1.8, (b) Ca/Si=0.8.

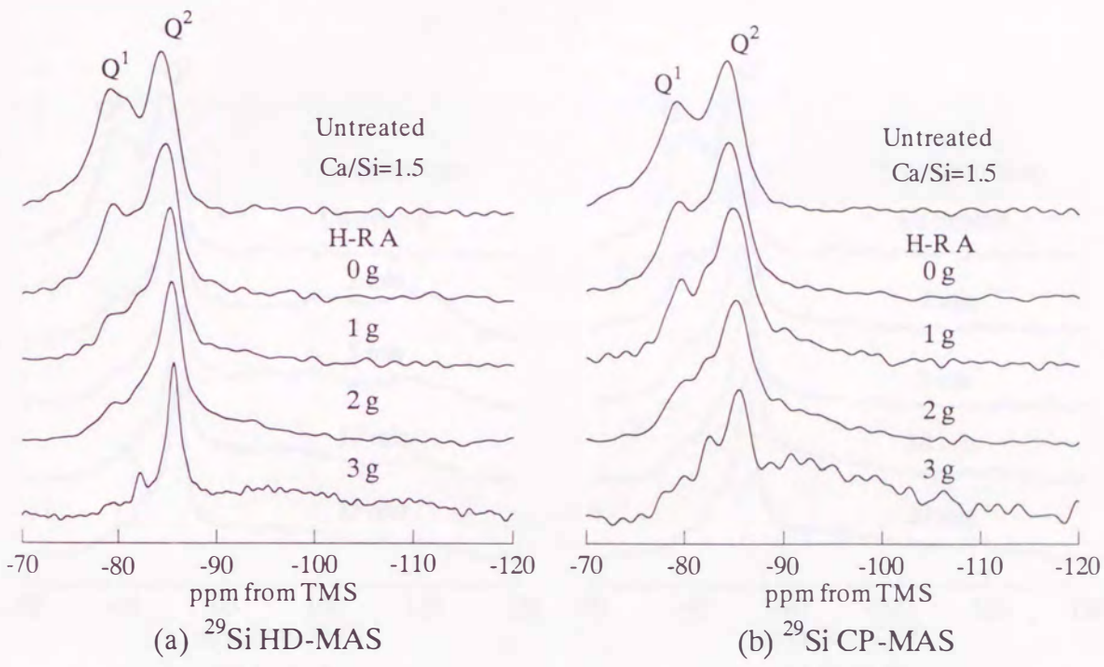

Figure 2.4 Variation of ^{29}Si MAS NMR spectra of C-S-H with a starting Ca/Si ratio of 1.5 treated by various quantities of H-R A for 2 hr. (a) HD-MAS, (b) CP-MAS.

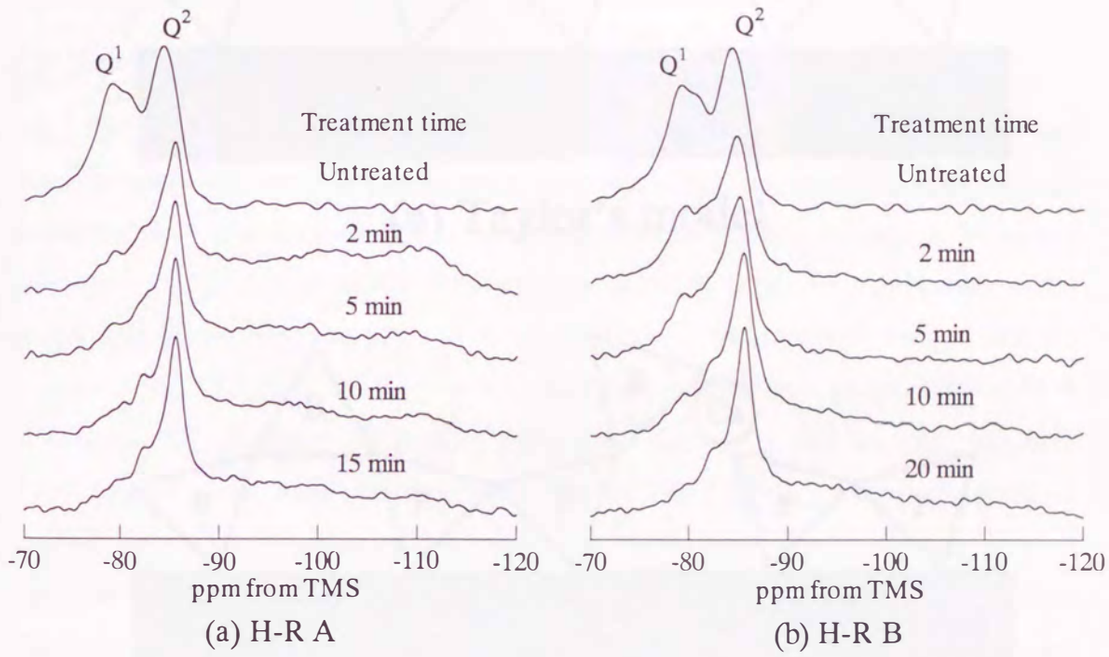

Figure 2.5 Variation of ^{29}Si HD-MAS NMR spectra of C-S-H with treatment time of H-type ion exchange resins. (a) H-R A, (b) H-R B.

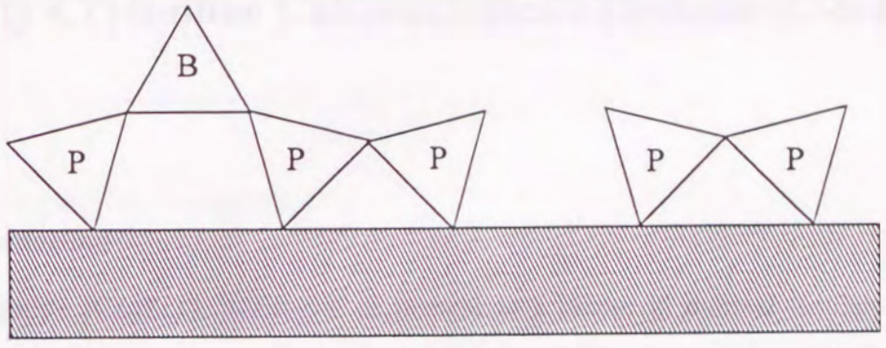

(a) Taylor's model

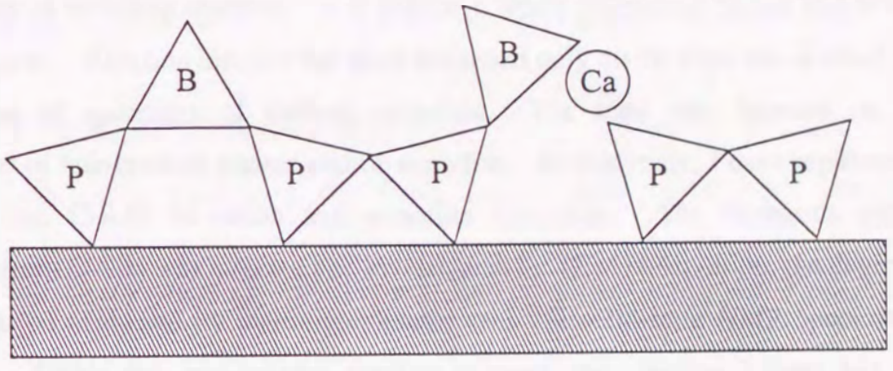

(b) Separation model by Ca^{2+}

Figure 2.6 Schematic structure models of C-S-H with a defect of dreier chain silicate anions. Shadowed plates denote Ca–O polyhedra, P and B denote paired and bridging Si–O tetrahedra, respectively. (a) Taylor's model [17], (b) Separation model by Ca^{2+}.

Chapter 3

Formation Mechanism of Xonotlite from Poorly-Crystalline Calcium Silicate Hydrate (C-S-H)

3.1 Introduction

Xonotlite [$Ca_6(Si_6O_{17})(OH)_2$] is of interest as a binder in thermal insulator and building materials. Its formation from lime and silica mixtures proceeds through intermediate phases such as C-S-H (poorly-crystalline calcium silicate hydrate) and tobermorite [11]. The formation mechanism of xonotlite is still unclear because of the complexity of multistep reaction. It is unknown where nucleation occurs and how the crystals grow. Reaction kinetics has been discussed only on the total rate derived from a decrease of quantities of starting materials. The total rate depends on both formations of intermediate phases and of xonotlite. In this study, I have separated the reaction into C-S-H formation and xonotlite formation. The formation step of xonotlite from C-S-H was targeted and investigated by TEM observation, the degrees of formation (α) evaluated by thermogravimetry, and ^{29}Si solid-state NMR spectroscopy [53, 54]. Using this step-by-step reaction method, the reaction system has been simplified and its microstructural change discussed more directly.

3.2 Experimental

3.2.1 Preparation of C-S-H

C-S-H was hydrothermally synthesized at 130 °C for 2 hr from CaO and silicic acid with a Ca/Si molar ratio of 1.0 in stirred suspension of a water/solid ratio of 40. The CaO was prepared by heating reagent grade $CaCO_3$ at 1000 °C for 4 hr. The silicic acid was amorphous silica of reagent grade with 20.8% ignition loss. First the CaO was added into 1/5 of total water and the suspension was vigorously stirred by a

ultradisperser for 2 min. Then silicic acid and the remaining water was added and stirred by the same manner again before autoclaving.

3.2.2 Formation of Xonotlite

After the preparation of C-S-H, the reaction temperature of an autoclave was increased in 15 min from 130 °C to 180, 200 or 220 °C, respectively and kept for certain times. Then the autoclave was quenched by a dip into water.

3.2.3 Examination of Products

The products were identified by XRD and TG (thermogravimetry) and the morphologies of the products were observed by TEM (transmission electron microscope). The products were filtered and dried under vacuum at 60°C for 2 days and then examined by XRD and TG. Specimens for TEM observation were prepared by rapid drying from methanol suspension of wet products just after filtration. This special drying method retains sample morphology well as shown in Figure 3.2.

3.2.4 Evaluation of Degrees of Formation

The degree of formation of xonotlite (α) was determined from TG loss around 800°C on the dehydration to wollastonite in terms of the following equation.

$$\alpha = (\Delta W - \Delta W_{CSH}) / (\Delta W_{Xo} - \Delta W_{CSH})$$

ΔW, ΔW_{CSH} and ΔW_{Xo} indicate TG losses (%) of the products, C-S-H and xonotlite, respectively. TG analyses were measured for 50 mg of a specimen by Rigaku TAS100 with a macro TG holder at 10°C/min. To neglect turbulence of TG at high temperatures, ΔW was identified as a difference at 700°C between the TG value and the value extrapolated from a straight line connecting TG points at 850 and 900°C, as illustrated in Figure 3.1. A mean value of 7 specimens containing only C-S-H, ΔW_{CSH}, was 1.24%. Although the theoretical value of ΔW_{Xo} is 2.52%, ΔW_{Xo} was assumed to be 2.30%, the value of a specimen formed at 200°C for 12 hr.

3.2.5 ^{29}Si NMR Measurement

All ^{29}Si NMR spectra were recorded on a Bruker AC200 (4.7 T magnetic field) at 39.7 MHz using cross polarization (CP) and magic angle spinning (MAS). The repetition time, the contact time (CT) and the spinning rate were 5 s, 4 ms and 3250 Hz, respectively. CP-MAS spectra of C-S-H and xonotlite were measured over the range of CT 0.5 to 5 ms. It was confirmed that Q^1, Q^2 and Q^3 signal intensities of CP-MAS at CT of 4 ms were almost equal to those of HD (high power decoupling) -MAS spectra within errors.

3.3 Results and Discussion

3.3.1 Characterization of C-S-H

The XRD of C-S-H exhibited relatively sharp reflections at 0.31, 0.28 and 0.18 nm. The TEM micrographs showed a homogeneous spread thin foil-like morphology (Figure 3.2 (a)), while crumpled foils (Figure 3.2 (b)) were observed by the vacuum-drying. These crumpled foils have been observed by many researchers but must be caused by drying. The spread foils are considered to be the real morphology in the reaction suspension. The concentrations of Ca and silicic acid in the quenched solution were 1.5 and 0.3 mmol·dm^{-3}, respectively. The Ca/Si molar ratio of C-S-H was estimated to be 0.99 from these concentrations.

3.3.2 TEM Observation

Figure 3.3 shows TEM micrographs and selected-area electron diffraction (SED) of the products formed in the process of formation of xonotlite at 200°C. There were stripes in the foils in the product (a) at reaction time of 45 min. The SED patterns (b) and (c) indicate the foils are C-S-H and the stripes are xonotlite. The stripes grew longer and thicker in foil-like C-S-H in (d) at 75 min. The foils disappeared in (e) and (f) at 2 hr. The TEM observation confirms that C-S-H prepared hydrothermally shows homogeneous foil-like morphology and the nucleation of xonotlite and its one-dimensional crystal growth occur in C-S-H.

3.3.3 Reaction Kinetics

The degrees of formation of xonotlite (α) were plotted against reaction time in Figure 3.4. Xonotlite was formed rapidly after a definite induction period at every reaction temperature.

The following general kinetic equation on the nucleation and growth model [59] was applied.

$$-\ln(1-\alpha) = k(t-t_0)^N$$

where α: degree of formation, t: reaction time, t_0: induction period, N :kinetic index.

From a plot of logarithms of each side of the above equation, the N value was obtained. It was near unity at every temperature as shown in Table 1. On the assumption N=1, the plots was obtained in Figure 3.5. From these plots, the kinetic parameters (t_0, k) and the correlation coefficients (γ) were obtained by the least-squares method as shown in Table 1. Apparent activation energy of nucleation [60] and that of growth in Table 1 were estimated by the Arrhenius's plots of $1/t_0$ and k, respectively. Nearly equal values indicate the similarity of the microstructural change of nucleation and that of growth.

According to Brown et al. [61], N=1 indicates one-dimensional phase-boundary controlled growth or two-dimensional diffusion-controlled growth with saturation of nucleation sites. The TEM observation supports one-dimensional crystal growth.

3.3.4 ^{29}Si NMR Spectra

CP-MAS NMR spectra of C-S-H and the products treated at 200°C are shown in Figure 3.6. C-S-H had only two signals, an end group Q^1 (–79.5 ppm) and a middle group Q^2 (–84.3 ppm), which corresponds to the single chain structure of silicate anions. After an induction period of 58 min, Q^2 signal became sharper and a signal of Q^3 (–97.6 ppm) appeared and, which corresponds to the formation of the double chain structure of xonotlite. The chemical shifts of Q^1, Q^2 and Q^3 of xonotlite were –79.6, –86.6 and –97.6 ppm, respectively. The variation of distribution of Q^1, Q^2, and Q^3 was plotted against the reaction time in Figure 3.7. Q^1 increased during the temperature increase and the induction period, while it decreased with the formation of xonotlite. Q^2 is a main component over the whole process. Q^3 increased with the formation of xonotlite.

3.3.5 Chemical Shift of Q^2

The chemical shift is caused by the variation of the electronic structure around ^{29}Si nucleus. Every remaining two bonds of Q^2 in xonotlite link to the Ca–O layer, while C-S-H has Si–OH groups. According to Janes and Oldfield [58], a signal shifts toward low-frequency by 0.43 ppm when Si–OH changes to Si–OCa. The chemical shift of Q^2 of C-S-H changed from –84.3 to –85.3 ppm during the induction period, which suggests some of Q^2 became well bonded to Ca–O layer and provides the origin of nuclei of xonotlite. The broadening of Q^2 signal during the same period indicates that the Si environment began to be inhomogeneous by the nucleation in C-S-H before developing the xonotlite structure.

3.3.6 Silicate Anion Chain Length

Variations of Q^2/Q^1, $(Q^2+Q^3)/Q^1$ and Q^3/Q^2 intensity ratios and the degrees of formation of xonotlite are shown in Figure 3.8. The mean chain length of silicate anions by Si–O tetrahedra unit can be estimated from $2\times(1 + Q^2/Q^1)$ for C-S-H and $2\times\{1 + (Q^2+Q^3)/Q^1\}$ for xonotlite. The mean silicate chain length was estimated to be 8 for the original C-S-H, decreased to 5 during the induction period and increased to 17 at 12 hr of reaction time. The Q^3/Q^2 ratios corresponded well to the degrees of the formation. The decrease of chain length during the induction period corresponds to the structural change of C-S-H due to nucleation of xonotlite.

3.4 Conclusions

Homogeneous C-S-H with a Ca/Si molar ratio of 1.0 was prepared hydrothermally at 130°C. Xonotlite is formed from C-S-H at 180, 200 and 220°C after a rapid increase of the reaction temperature. The formation process of xonotlite from C-S-H was investigated by TEM observation, the degree of formation (α) evaluated by thermogravimetry, and ^{29}Si solid-state NMR spectroscopy.

1) The TEM observation confirms that C-S-H prepared hydrothermally shows homogeneous foil-like morphology and the nucleation of xonotlite and its one-dimensional crystal growth occurs in the C-S-H.

2) The analysis of the formation rate based on the nucleation and growth model suggests that the one-dimensional phase-boundary controlled growth be in accord with the TEM observation.

3) The apparent activation energy of nucleation and that of growth were almost the same values, 118 and 111 $kJ \cdot mol^{-1}$, respectively.

4) The chemical shift of ^{29}Si NMR of middle groups Q^2 of C-S-H changed from –84.3 to –85.6 ppm during the induction period of xonotlite formation, which suggests some of Q^2 became well bonded to Ca–O layer and is the origin of nuclei of xonotlite crystals. The mean chain length of silicate anions was estimated from Q^2/Q^1 and $(Q^2+ Q^3)/Q^1$ intensity ratios. The mean silicate chain length decreased during the induction period and increased with formation of xonotlite.

Table 3.1 N (kinetics index), induction periods (t_0), rate constants (k), correlation coefficients (γ) and apparent activation energies of nucleation (ΔE_a^N) and growth (ΔE_a^G).

Temp. / °C	N	t_0 / min	k /10^{-3}min^{-1}	γ	ΔE_a^N / kJ·mol^{-1}	ΔE_a^G / kJ·mol^{-1}
180	0.82	199	6.11	0.985		
200	0.89	57.6	23.4	0.997	118	111
220	1.11	15.8	67.1	0.989		

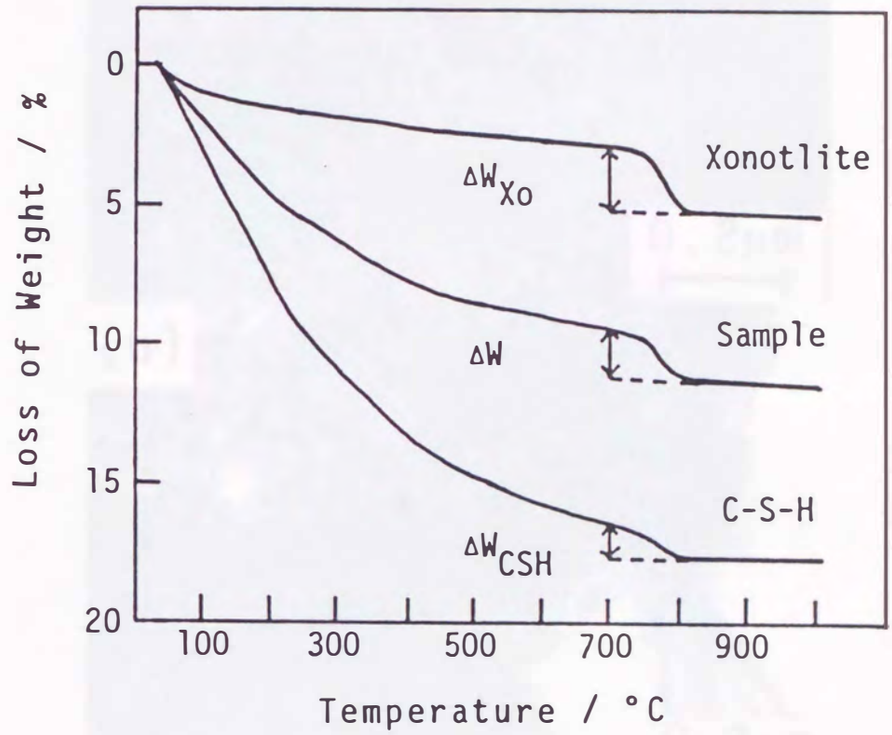

Figure 3.1 Thermogravimetry of C-S-H , sample and xonotlite. C-S-H was prepared at 130°C for 2 hr. Xonotlite was synthesized at 130°C for 2 hr and 200°C for 12 hr.

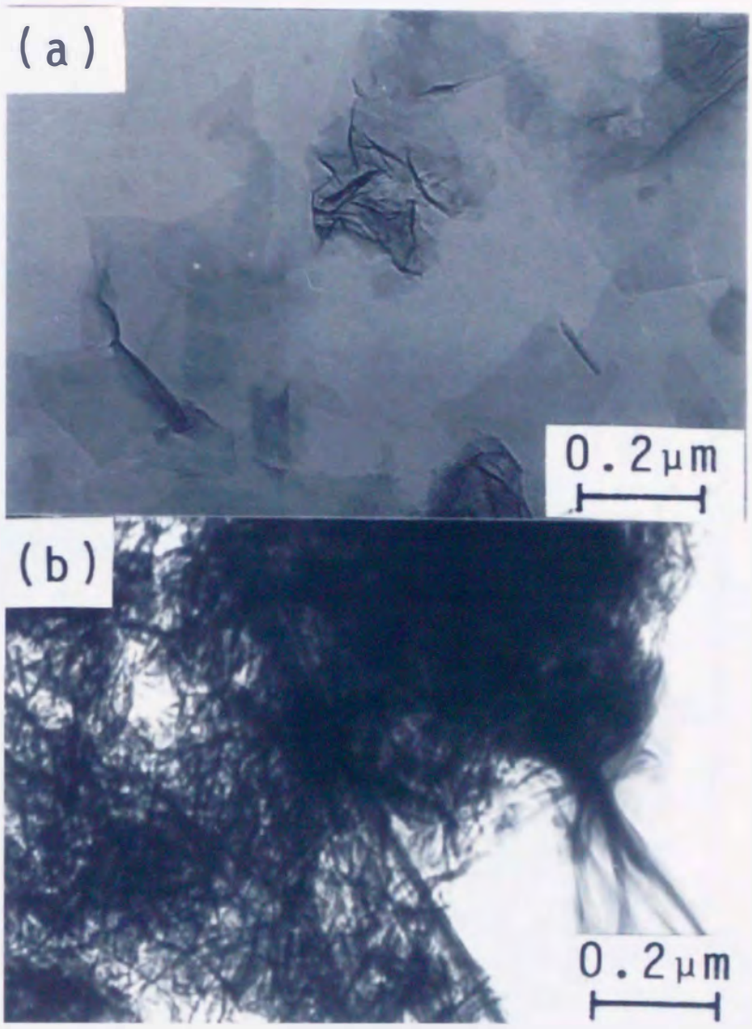

Figure 3.2 TEM photographs of C-S-H.
(a): sample rapidly dried, (b): sample vacuum-dried for 2 days at 60°C.

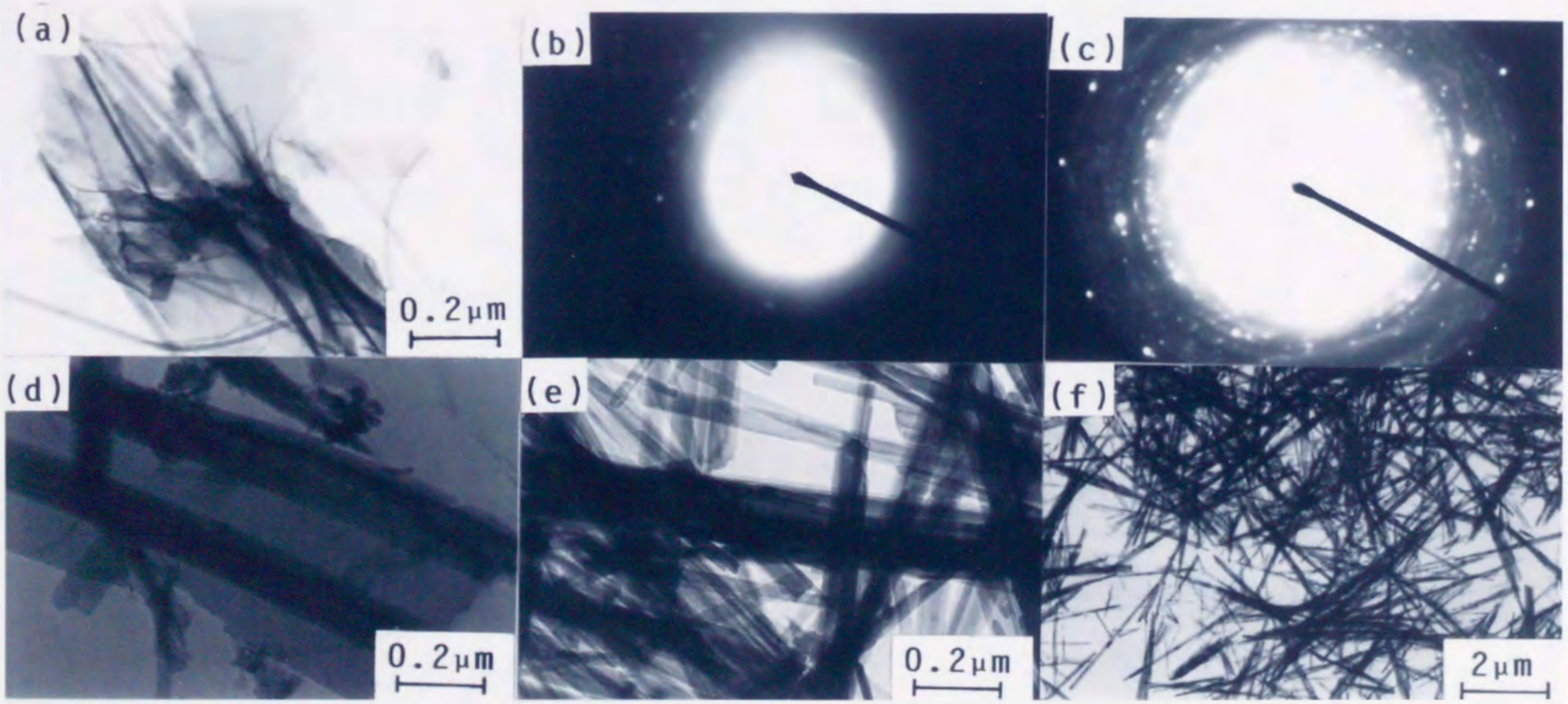

Figure 3.3 TEM and SED (Selected-area Electron Diffraction) photographs of the products in the process of formation of xonotlite at 200°C. (a): sample at reaction time of 45 min, (b): SED pattern of foil-like part of (a), (c): SED pattern of lath-like part of (a), (d): sample at reaction time of 75 min, (e), (f): sample at reaction time of 12 hr.

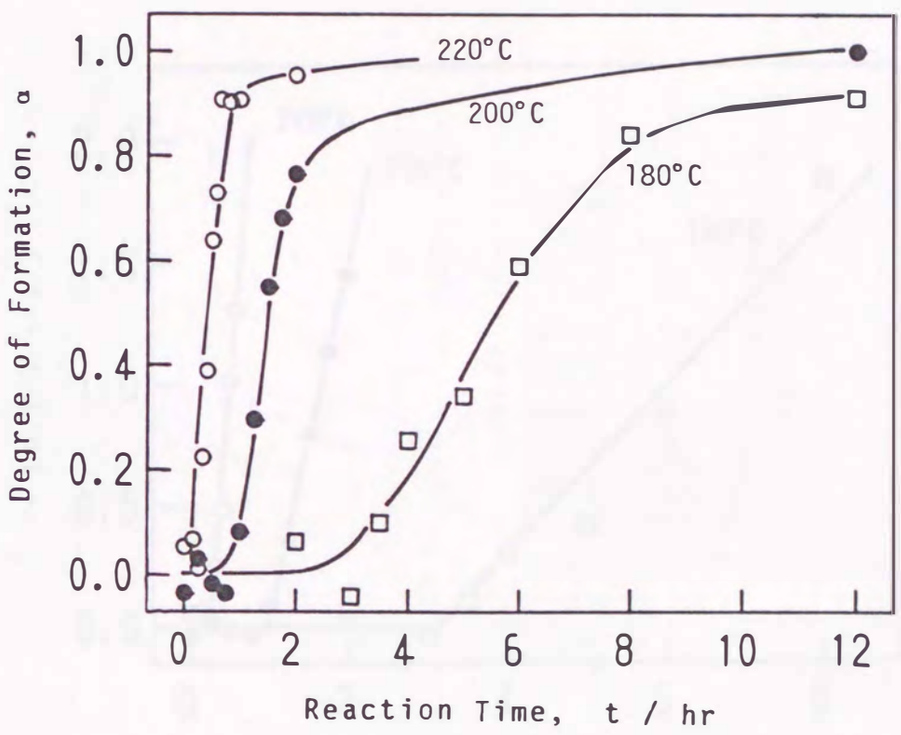

Figure 3.4 Variation of the degree of formation of xonotlite determined by thermogravimetry.

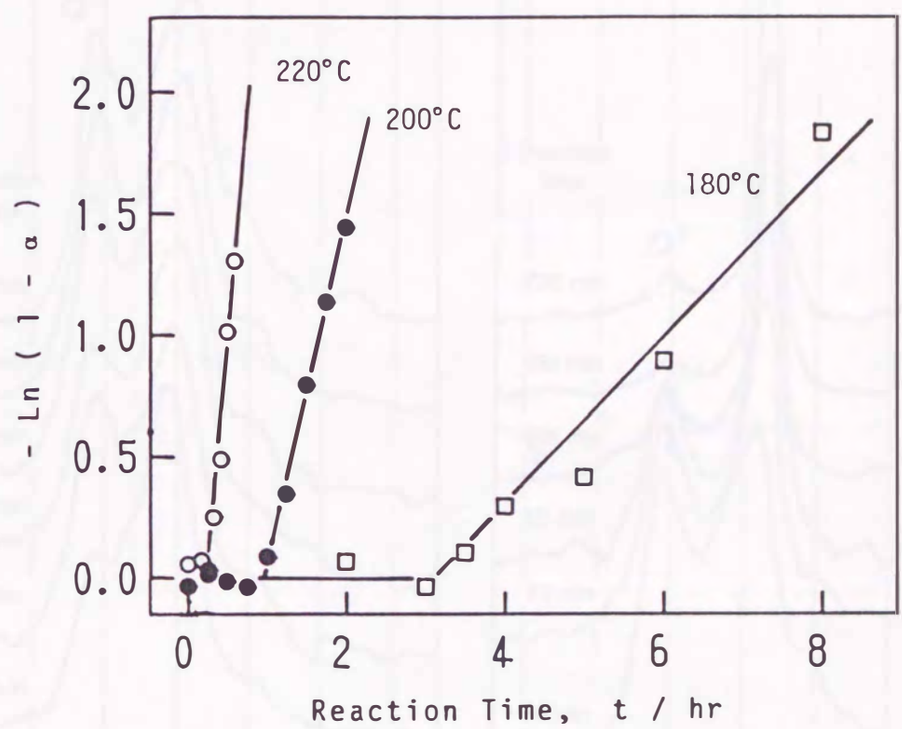

Figure 3.5 Variation of – Ln(1–α) with reaction time.

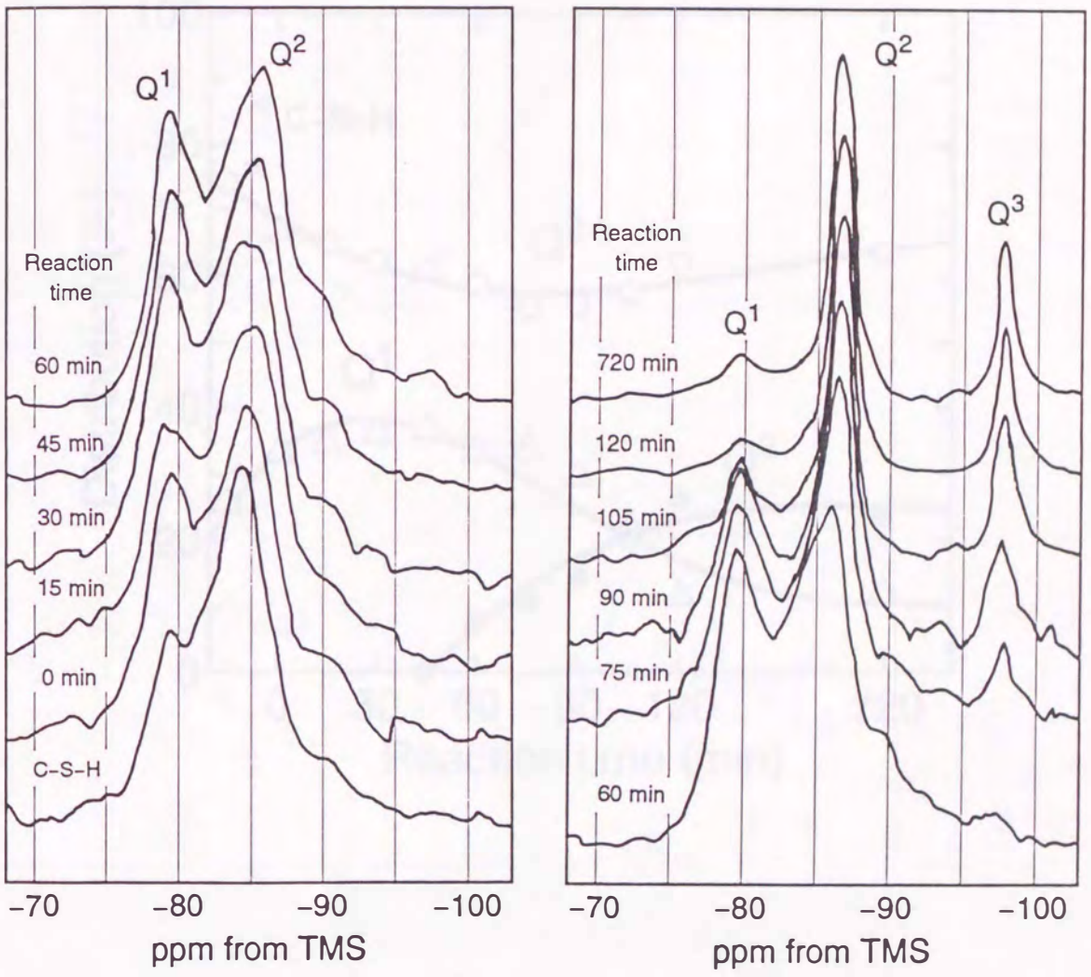

Figure 3.6 CP-MAS NMR spectra of C-S-H and the products treated at 200°C from 0 to 720 min.

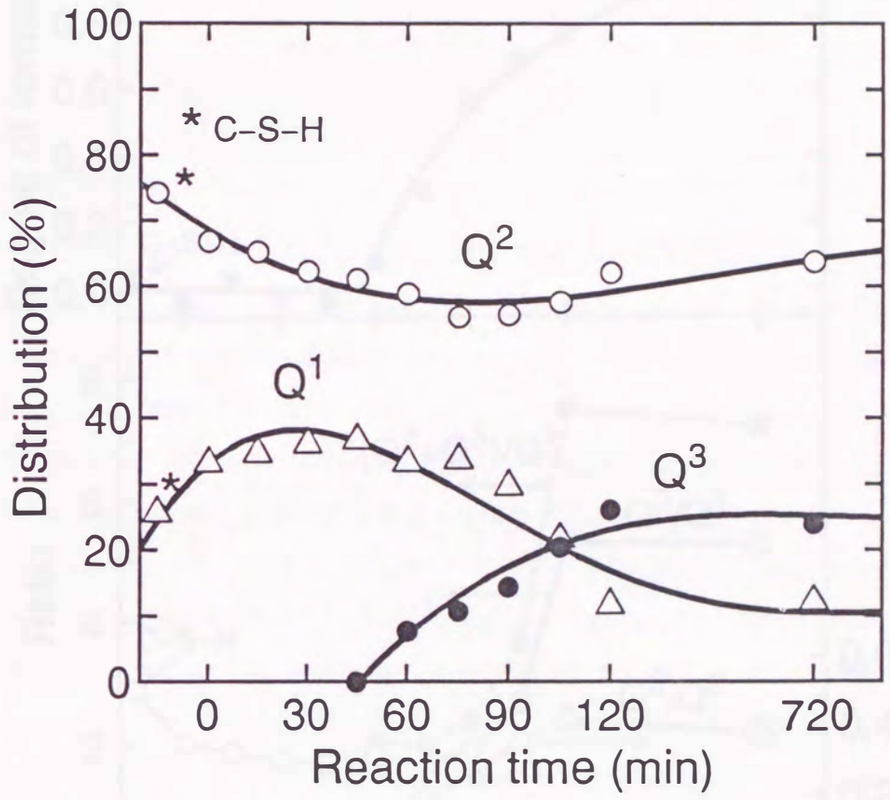

Figure 3.7 Variation of distribution (%) of Q^1, Q^2 and Q^3 from CP-MAS NMR spectra of C-S-H and products at 200°C with reaction times.

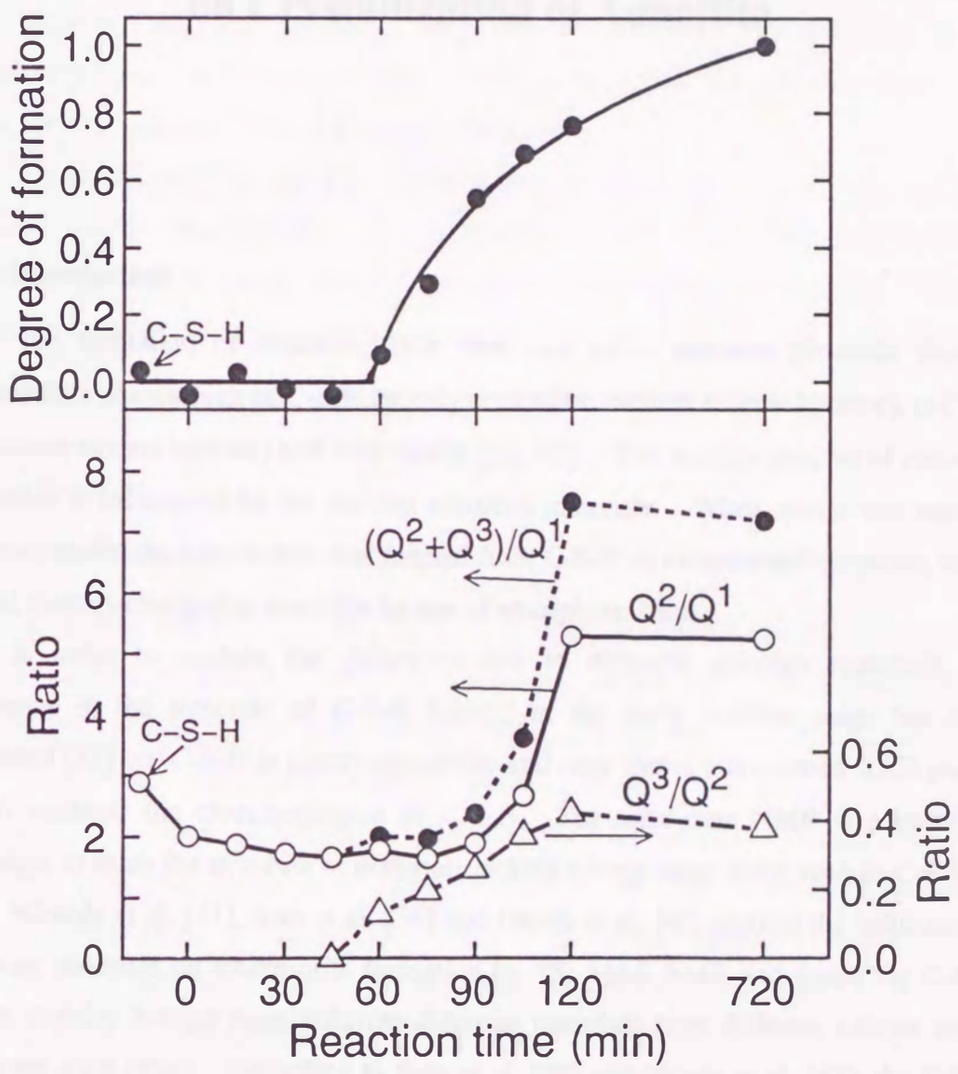

Figure 3.8 Variation of NMR signal intensity ratios and degrees of formation of xonotlite at 200°C with reaction times.

Chapter 4
Influence of Siliceous Materials on Crystallization of Xonotlite

4.1 Introduction

The formation of xonotlite from lime and silica mixtures proceeds through intermediate phases such as C-S-H (poorly crystalline calcium silicate hydrate), α-C_2SH (dicalcium silicate hydrate) and tobermorite [11, 62]. The reaction process of xonotlite formation is influenced by the starting siliceous materials. When quartz was used as siliceous materials, tobermorite was formed from C-S-H as an intermediate phase, while C-S-H directly changed to xonotlite by use of amorphous silica.

In order to explain the difference due to different siliceous materials, the difference in the structure of C-S-H formed in the early reaction stage has been suggested [12] but C-S-H is poorly crystalline and only shows a few broad XRD peaks, which inhibited the characterization of C-S-H. The solid-state NMR is a powerful technique to study the structure of materials lacking a long-range order such as C-S-H.

Mitsuda et al. [41], Sato et al. [38] and Okada et al. [43] studied the influence of siliceous materials on tobermorite formation by ^{29}Si MAS NMR and found the C-S-H phases initially formed from different siliceous materials have different silicate anion structures each other. According to Sato et al. [38] and Okada et al. [43], the C-S-H form quartz showed a low Q^2/Q^1 intensity ratio, which suggested that the C-S-H contained short silicate chains and dimers. The C-S-H formed from amorphous silica had a high Q^2/Q^1 intensity ratio and a Q^3 peak, which indicates the presence of long and cross-linked silicate chains. They concluded that the C-S-H from amorphous silica was hard to crystallize to tobermorite due to the presence of a long and cross-linked

silicate chains and that the C-S-H from quartz easily crystallized due to its short silicate chain structure.

Tobermorite is hydrothermally synthesized from silica and lime mixture in the same manner as xonotlite. The Ca/Si ratio of tobermorite is 0.83 lower than that of xonotlite, 1.0, and tobermorite is hydrothermally synthesized ordinarily at lower temperatures, about 180 °C, than xonotlite, about 200 °C. The difference in the hydrothermal reaction conditions between formations of xonotlite and tobermorite may affect the structure of C-S-H as an intermediate phase.

The xonotlite formation process using various siliceous materials have not been analyzed by ^{29}Si MAS NMR. In this chapter, I applied the ^{29}Si MAS NMR to determine the early intermediates in the xonotlite formation and clarified the influence of starting siliceous materials on the xonotlite formation using 4 kinds of siliceous materials.

4.2 Experimental

4.2.1 Raw Materials

As for siliceous materials, two kinds of rice husk ashes with different crystallinity (RHA-amorphous and RHA-crystal) and two kinds of quartz sand with different particle size distribution (Quartz-fine and Quartz-coarse). The physico-chemical properties of the siliceous materials are summarized in Table 4.1 [62].

RHA-amorphous was prepared by burning rice husk produced in Saga prefecture on an iron plate and heating in an electric furnace at 600 °C. RHA-amorphous was gray and composed of amorphous silica. It was very porous because it maintained the morphology of the cell structure of rice husk, which was confirmed by the SEM observation [62]. RHA-crystal was obtained by burning rice husk piled up in open-field in Malaysia [63]. RHA-crystal was pinkish and composed of cristobalite and tridymite. The porous structure of rice husk was destroyed and its BET specific surface area (2.5 m^2/g) was much smaller than that of RHA-amorphous (20.5 m^2/g). The rice husk ashes were crashed by a ball-mill with cyclohexane and dried. The quartz sands were crashed by a boll mill under a dry condition and their particle sizes

were controlled with a time of milling. The Blaine specific surface areas of Quartz-fine and Quartz-coarse were 6770 and 3190 cm^2/g, respectively.

CaO was obtained by heating reagent grade $CaCO_3$ at 1100 °C for 4 hours.

4.2.2 Formation of Xonotlite

CaO and siliceous material with Ca/Si molar ratios of 1.0 were mixed with water at a water/solid ratio of 40 in an autoclave. The autoclave was heated up to 190 °C at 2 °C/min and then kept at this temperature from 0 to 8 hr with stirring at 200 rpm. After quenching the autoclave, the products were filtered and vacuum-dried at 60 °C for 2 days.

4.2.3 ^{29}Si NMR and XRD Measurements

All ^{29}Si NMR spectra were recorded on a Bruker AC200 (4.7 T magnetic field) at 39.7 MHz by use of high power decoupling (HD) or cross polarization (CP) with magic angle spinning (MAS) of 3250 Hz. HD-MAS spectra were acquired with a repetition time of 10 s, the use of $\pi/4$ pulses (2.5 μs) and an accumulation number of 4096 and plotted with a line broadening factor of 30 Hz. For CP-MAS spectra, the repetition time, the contact time (CT), the accumulation number and the line broadening factor were 5 s, 2 ms, 1024 and 30 Hz, respectively. The chemical shifts were referenced to TMS by use of 3-(trimethylsilyl)-propane sulfonic acid sodium salt (DSS) as a secondary reference (1.53 ppm).

XRD powder patterns were recorded with Cu $K\alpha$ radiation on Rigaku RAD-II A. A 0.02° of 2θ step size and 1-second count time were used.

4.3 Results and Discussion

4.3.1 XRD Patterns

The XRD patterns of the products formed from RHA-amorphous are shown in the Figure 4.1. The pattern of the product at 0 hr consists of relatively sharp reflections at 0.18 nm (2θ = 49.6°), 0.28 nm (31.9°) and 0.30 nm (29.3°). This is the same pattern of C-S-H at C/S ratio of 1.0 shown in Figure 2.1. Non-reacted $Ca(OH)_2$ and silica were

not detected. This C-S-H was stable and showed the same XRD pattern below the reaction time of 4hr. The peaks of xonotlite appeared only after 4 hr. The results in Chapter 3 suggest that C-S-H change directly to xonotlite. In Chapter 3, C-S-H was synthesized from amorphous silica.

The XRD patterns of the products from RHA-crystal are shown in the Figure 4.2. At a reaction time of 0 hr, only the pattern of C-S-H is observed just like RHA-amorphous. The peaks were, however, very broad compared with those of C-S-H from RHA-amorphous. The broadness of the peaks indicates the distortion of the Ca-O layer, because the reflection peaks of C-S-H correspond to the important repeat distance of the Ca–O layer structure [17]. Therefore, the C-S-H from RHA-crystal must have a more distorted structure compared with the C-S-H from RHA-amorphous. The structure of C-S-H depends on the starting siliceous materials. 1.1 nm tobermorite was formed at 2 hr and disappeared at 6 hr. On the other hand, xonotlite was formed after 4 hr. Taylor [64] reported that the topotactic transformation of natural 1.1 nm tobermorite into xonotlite using single crystal X-ray method. Mitsuda et al. [11] confirmed by the TEM observation that the plate- or lath-like tobermorite decomposed into fibrous xonotlite. Therefore, xonotlite is considered to be directly changed from tobermorite.

The XRD patterns of the products from Quartz-fine are shown in the Figure 4.3. At the reaction time of 0 hr, there remained a large amount of non-reacted $Ca(OH)_2$ and quartz. A broad peak near 30 ° was also observed at 0 and 1 hr. This indicates the formation of C-S-H. At the reaction time of 1 hr, the pattern of C-S-H becomes clear with a small amount of quartz. The C-S-H pattern is the same as the C-S-H obtained from RHA-crystal. After the reaction time of 2 hr, the XRD pattern changed in the same manner as RHA-crystal. The similarity of the reaction processes between Quartz-fine and RHA-crystal must be caused by the similarity of the structure of the C-S-H formed from both siliceous materials in the early stage.

The XRD patterns of the products from Quartz-coarse are shown in the Figure 4.4. At the early reaction stage, α-C_2SH (α-dicalcium silicate hydrate) $Ca_2(SiO_4H)(OH)$ was formed instead of C-S-H and remained until 6 hr. C-S-H was formed after a reaction time of 4 hr. Because plate-like α-C_2SH crystals was covered

by fibrous C-S-H at 4 hr according to SEM observation [62], α-C_2SH seems to decompose to form C-S-H as the dissolution of quartz proceeded. Finally a small amount of xonotlite was formed only at reaction time of 8 hr. There remained non-reacted quartz until a reaction time of 4 hr.

The reaction process of each siliceous material is summarized in Table 4.2. Using RHA-amorphous as siliceous material, C-S-H was formed and directly changed to xonotlite in the same manner as described in Chapter 3. The reaction for RHA-crystal and Quartz-fine proceeded the same manner. The C-S-H formed in the early stage from both crystalline siliceous materials has distorted Ca-O structure compared with the C-S-H from RHA-amorphous. The C-S-H changed to 1.1 nm tobermorite and then tobermorite decomposed to form xonotlite. The product first formed from Quartz-coarse was α-C_2SH and decomposed to C-S-H and finally xonotlite was formed. Therefore, it is concluded that the products formed in the early stage determine the reaction process.

4.3.2 ^{29}Si NMR Spectra

The ^{29}Si HD-MAS and CP-MAS NMR spectra of the products from RHA-amorphous are shown in Figure 4.5. A relatively sharp Q^1 and Q^2 signals were observed at the reaction time of 0 hr when only C-S-H was produced. These signals were in accord with the signals of C-S-H with Ca/Si ratio of 1.0 formed from amorphous silica in Figure 2.2 in Chapter 2. The Q^2 signal showed a shoulder at –82 ppm, which is the Q^2_H shown Figure 2.3. During the reaction time from 0 to 6 hr, the Q^2 signal becomes broader and shows lower-frequency shift. These variations of Q^2 signal were also observed in Figure 3.6 in Chapter 3. After 4 hr the Q^3 signal at –97.5 ppm appeared with xonotlite formation.

The ^{29}Si HD-MAS and CP-MAS NMR spectra of the products from RHA-crystal are shown in Figure 4.6. In the HD-MAS spectrum at the reaction time of 0 hr, Q^1 at –79 ppm and Q^2 at –85 ppm and a broad signal between –90 and –100 ppm were observed. The broad signal was considered to be the Q^2_L signal in Figure 2.3, which was observed for C-S-H with Ca/Si ratio < 1.0. At the reaction time of 2 hr, when tobermorite was formed, the Q^2 signal of HD-MAS shows a higher frequency shift and

the broad line between –90 and –100 ppm increases. The Q^3 signal of 1.1 nm tobermorite in the range between –96 and –97 ppm [34, 41] was not detected. At a longer reaction time than 4 hr, when xonotlite also formed, the Q^3 signal of xonotlite at –97.5 ppm appeared in both the HD-MAS and the CP-MAS spectra.

The HD-MAS spectra at the reaction time of 0 hr in Figures 4.5 and 4.6 were much different. Only C-S-H was detected by XRD in Figures 4.1 and 4.2 and neither non-reacted $Ca(OH)_2$ nor silica was observed. Therefore, the total Ca/Si ratios of both C-S-H from RHA-amorphous and RHA-crystal must be 1.0. The difference in HD-MAS NMR signals in Figures 4.5 and 4.6 corresponds to the difference observed in XRD patterns in Figure 4.1 and 4.2.

The ^{29}Si HD-MAS and CP-MAS NMR spectra of the products from Quartz-fine are shown in Figure 4.7. At the reaction time of 0 hr, a large amount of non-reacted $Ca(OH)_2$ and quartz remained as mentioned earlier. A large signal intensity of Q^1 in HD-MAS and CP-MAS was observed. This indicates that the silicate chains of the C-S-H formed are shorter than those of C-S-H from RHA-amorphous. The Ca/Si ratio of the C-S-H from Quartz-fine is higher than 1.0 because the remaining of a large amount of non-reacted quartz. This remaining quartz was not observed in HD-MAS and CP-MAS spectra because a repetition time of 10 s of HD-MAS is too short for a relaxation of ^{29}Si nuclear spins in quartz and quartz has no protons which are necessary for CP enhancement. After the reaction time of 1 hr, the HD-MAS and CP-MAS spectra becomes similar to those of the products from RHA-crystal shown in Figure 4.6. Q^1 becomes smaller and a broad signal between –90 and –100 ppm was observed. The similarity of the NMR signal of both C-S-H from RHA-crystal and Quartz-fine in Figure 4.6 and 4.7 corresponds to the similarity of those XRD patterns in Figure 4.2 and 4.3. At the reaction time of 2 hr, the broad signal of HD-MAS increased and two sharp signals at –92 ppm and –96 ppm appeared in CP-MAS. The signal at –92 ppm had been observed in the process of tobermorite formation and assigned to Q^2 by Sato et al. [38] and Okada et al. [43] and the signal at –96 ppm is the Q^3 of 1.1 nm tobermorite. After 4 hr, when tobermorite changed to xonotlite, the broad signal in HD-MAS and the signal at –92 ppm in CP-MAS disappeared and the signal at –97 ppm of Q^3 of xonotlite increased in both HD-MAS and CP-MAS.

The ^{29}Si HD-MAS and CP-MAS NMR spectra of the products from Quartz-coarse are shown in Figure 4.8. At a reaction time of 2 hr, only one sharp signal at –72.1 ppm was observed. This signal is assigned to the Q^0 unit of α-C_2SH (α-dicalcium silicate hydrate) [37]. The remaining quartz was not observed in HD-MAS and CP-MAS spectra because of the above-mentioned reason. After 4 hr, the signals of α-C_2SH decreased and the signals of Q^1 and Q^2 of C-S-H appeared. The signal at –97 ppm of Q^3 signal of xonotlite first appeared at 8 hr.

4.3.3 Reaction Mechanism

The reaction process varies with siliceous materials as summarized in Table 4.2. The C-S-H formed in the early stage from RHA-crystal and Quartz-fine shows the much different XRD pattern and NMR signals from those of C-S-H formed from RHA-amorphous. The C-S-H from RHA-crystal and Quartz-fine changed to tobermorite and then xonotlite was formed, while the C-S-H from RHA-amorphous directly changed to xonotlite in the same manner of the reaction process examined in detail in Chapter 3. The product formed in the early stage from Quartz-coarse was α-C_2SH. This changed to C-S-H and finally xonotlite was formed. In conclusion, the products formed in the early stage are considered to determine the next reaction stage.

I considered that the rate of dissolution of each siliceous material is important to determine the reaction process [62]. The reaction of CaO and silica proceeds in the inhomogeneous system of solid and solution. CaO change to $Ca(OH)_2$ and the solubility of $Ca(OH)_2$ is much higher than that of silica below 100 °C. Therefore, the rate of dissolution of the siliceous materials determines the products in the early stage of the reaction. Considering the difference in the processes from Quartz-fine and Quartz-coarse, it is clear that not only the solubility of the siliceous materials but the rate of dissolution is important.

The solubility of silica in water at 200 °C is 949 ppm for amorphous silica [65], 454 ppm for cristobalite [66], 265 ppm for quartz [66]. The order of the BET specific surface areas of the siliceous materials used in this study is RHA-amorphous > RHA-crystal ~ Quartz-fine > Quartz-coarse as show in Table 4.1. Therefore, the order of the rate of dissolution of the silica is considered to be RHA-amorphous $\gg$ RHA-crystal >

Quartz-fine ≫ Quartz-coarse. RHA-crystal and Quartz-fine have the similar rate of dissolution and they showed the same reaction process. This indicates that the reaction process highly depends on the rate of dissolution of the siliceous materials.

Considering the difference in the rate of dissolution of the siliceous materials, the difference in the products formed in the early stage can be understood as follows.

RHA-amorphous is expected to have the highest rate of dissolution. Silica was dissolved easily and the product at the reaction time of 0 hr had non-reacted silica. The C-S-H produced from RHA-amorphous must be homogeneous as shown in the Chapter 3. The C-S-H has relatively long silicate chains and non-distorted Ca-O layers. This kind of C-S-H was relatively stable even at 190°C where xonotlite must be the most stable phase with Ca/Si ratio of 1.0. According to Sato et al. [38] and Okada et al. [43], the C-S-H formed in the early stage from amorphous silica had a high Q^2/Q^1 intensity ratio and a Q^3 peak, which indicates the presence of long and cross-linked silicate chains. They concluded that the C-S-H from amorphous silica was hard to crystallize to tobermorite due to the presence of a long and cross-linked silicate chains. In our system the C-S-H formed in the early stage showed the sharp Q^1 and Q^2 signals but did not show the broad Q^3 signal. It is mainly because the Ca/Si ratio of xonotlite formation system is higher than that of tobermorite formation. On the contrary to the results of Sato et al. [38] and Okada et al. [43], the C-S-H in our system did not have cross-linked silicate chains. Therefore, tobermorite formation was not inhibited due to the cross-linked silicate chains.

RHA-crystal and Quarts-fine has a medium rate of dissolution among those siliceous materials. In the earliest stage, C-S-H with Ca/Si ratio > 1.0 was formed, which has a large amount of Q^1 as shown in Figure 4.7. The chain length is shorter than the C-S-H from RHA-amorphous. Later the Ca/Si ratio of C-S-H becomes 1.0 but its structure was much different from the C-S-H from RHA-amorphous. It is mainly because that the Ca-O layer of the C-S-H formed in the early stage was much distorted. The Q^1 signal was small and a broad signal between –90 and –100 ppm (Q^2_L) was observed. This broad signal changed to Q^3 signal of tobermorite as seen in Figure 4.6 and 4.7. Therefor, this broad signal must be closely related to the structure

of tobermorite. Sato et al. assigned this signal to the bridging tetrahedra that are connected by hydrogen bonding and change to Q^3 of tobermorite [38].

The rate of dissolution of amorphous silica like RHA-amorphous is so fast. Therefore, most of silica is consumed before the temperature of an autoclave reaches the temperatures where tobermorite is more stable than C-S-H. While a part of silica of RHA-crystal and Quartz-fine remains at these temperatures. It is considered that this remaining silica tends to make a tobermorite-like structure.

The rate of dissolution of Quartz-coarse is slow. Therefore, the Ca/Si ratio of the hydrothermal solution must be appropriate for the formation of α-C_2SH.

4.4 Conclusions

The influence of the siliceous materials on the xonotlite formation was studied using 4 kinds of siliceous materials. The siliceous materials were two kinds of rice husk ash with different crystallinity (RHA-amorphous, RHA-crystal) and two kinds of silica sand with different particle size distribution (Quartz-fine, Quartz-coarse). RHA-amorphous was composed of amorphous silica and RHA-crystal was composed of cristobalite and tridymite. The Blaine specific surface areas of Quartz-fine and Quartz-coarse were 6770 and 3190 cm^2/g, respectively. To study the reaction process, the reaction time was changed from 0 to 8 hr at 190°C. The products were identified by XRD and analyzed by ^{29}Si MAS NMR.

1) The order of the rate of dissolution of siliceous materials was considered in terms of solubility and specific surface area as follows; RHA-amorphous $\gg$ RHA-crystal > Quartz-fine $\gg$ Quartz-coarse. The reaction process was highly dependent on the rate of dissolution of siliceous materials.
2) The products formed in the early stage of the reaction vary with siliceous materials and determine the reaction process.
3) The C-S-H formed from RHA-amorphous has relatively sharp XRD peaks and NMR signals of Q^1 and Q^2. This C-S-H directly changes to xonotlite.
4) The C-S-H formed from RHA-crystal and Quartz-fine has a broad XRD pattern and a broad Q^2 signal between –90 and –100 ppm in addition to the Q^1 and Q^2

signals observed in the C-S-H from RHA-amorphous. This C-S-H easily changed to tobermorite and next xonotlite is formed.

5) α-C_2SH is formed from Quartz-coarse and changed to C-S-H and to xonotlite.

Table 4.1 Physico-chemical properties of siliceous materials.

Siliceous material	crystallinity	BET m^2/g	Blaine cm^2/g	lg. loss	SiO_2	Al_2O_3	K_2O
RHA-amorphous	amorphous	20.5	--	4.18	91.69	0.14	2.54
RHH-crystal	cristobalite trydimite	2.5	--	0.94	95.64	0.14	1.87
Quartz-fine	α-quartz	2.1	6770	0.38	98.13	1.16	0.14
Quartz-coarse		0.5	3190				

Table 4.2 Reaction process of xonotlite formation from siliceous materials

Siliceous material	Phase formed
RHA-amorphous	CSH → CSH, Xo → Xo → Xo
RHA-crystal	CSH → CSH, To → To, Xo → Xo
Quartz-fine	CSH → CSH, To → To, Xo → Xo
Quartz-coarse	C_2SH → C_2SH, CSH → CSH, Xo → Xo

CSH: C-S-H, C_2SH: α-C_2SH, Xo: xonotlite, To: 1.1 nm tobermorite.

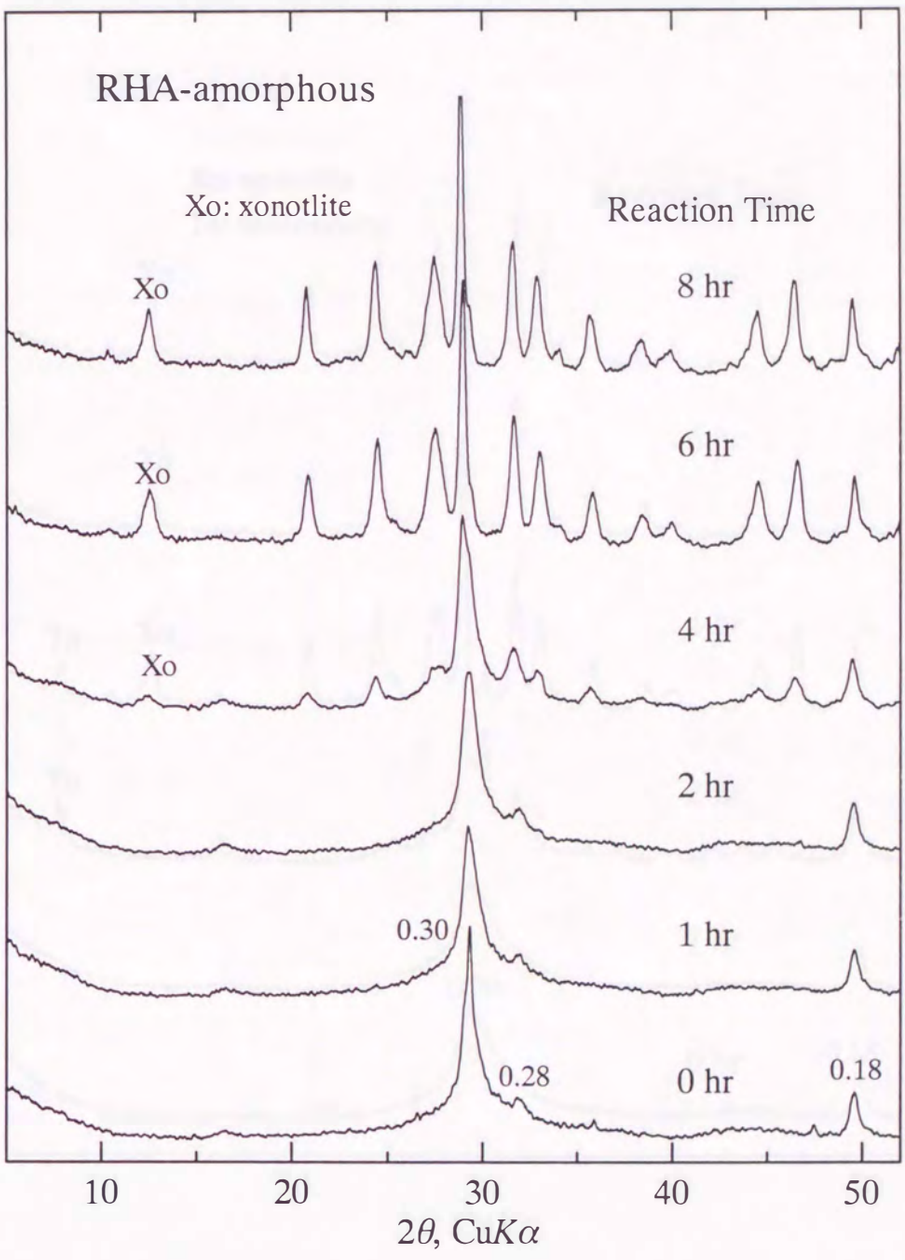

Figure 4.1 XRD patterns of the products hydrothermally synthesized from RHA-amorphous.

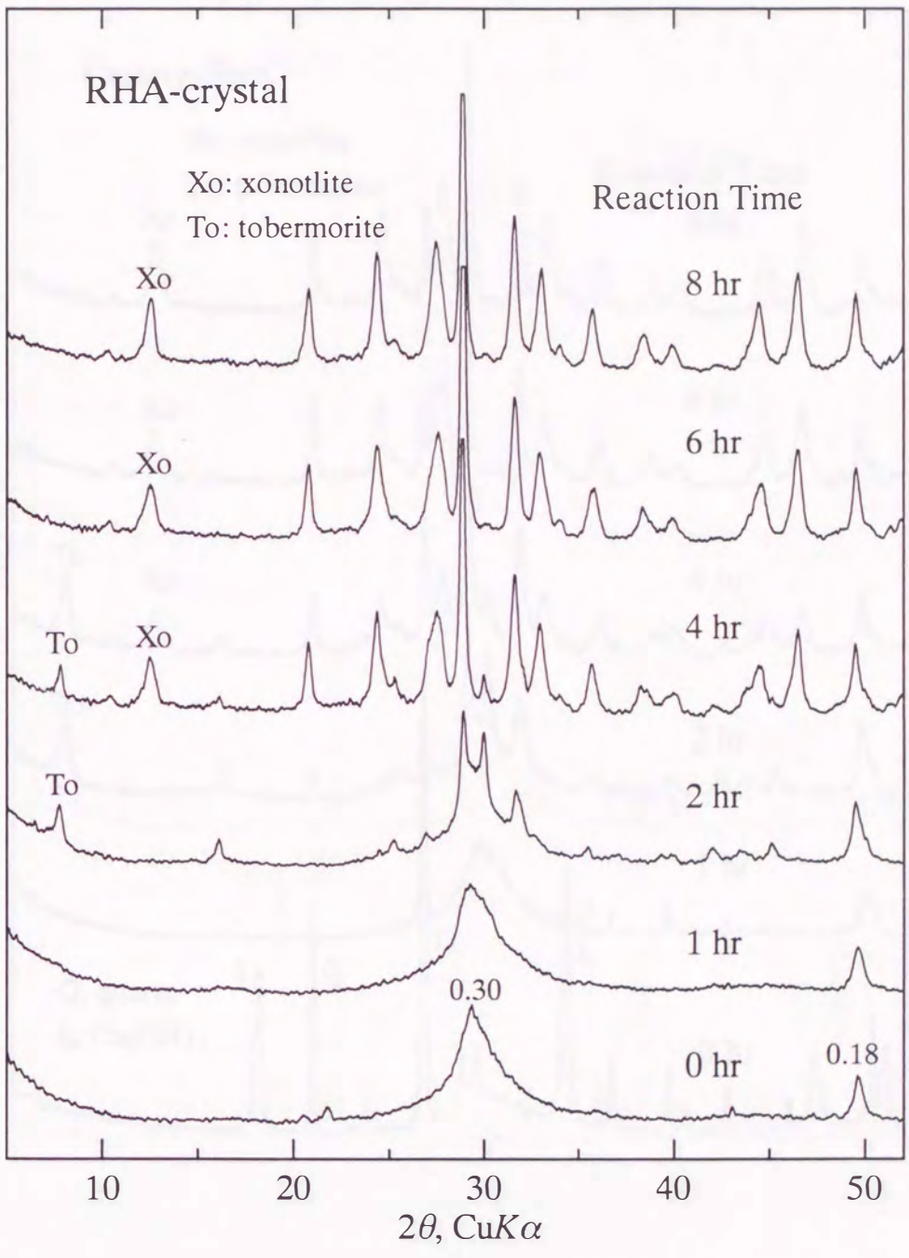

Figure 4.2 XRD patterns of the products hydrothermally synthesized from RHA-crystal.

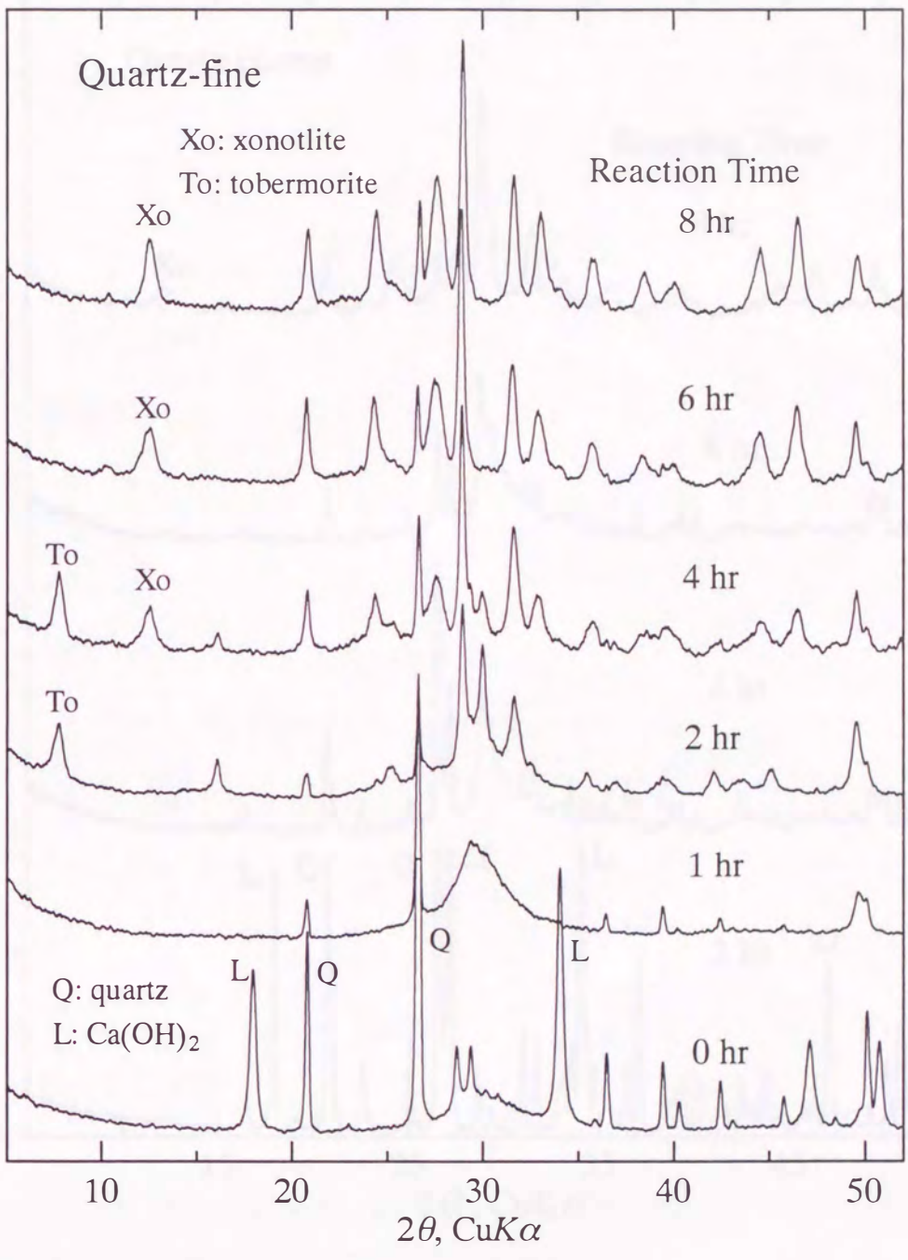

Figure 4.3 XRD patterns of the products hydrothermally synthesized from Quartz-fine.

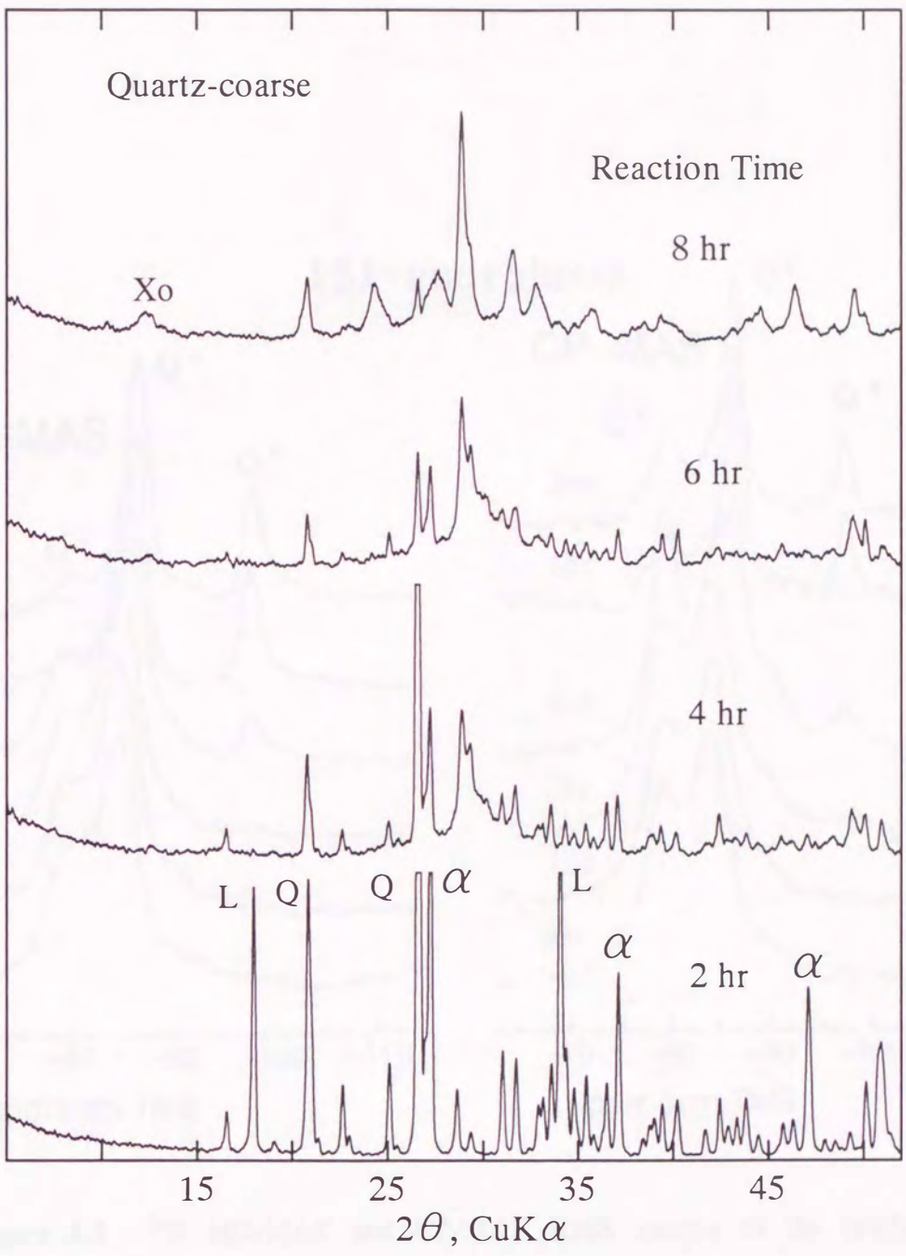

Figure 4.4 XRD patterns of the products hydrothermally synthesized from Quartz-coarse.

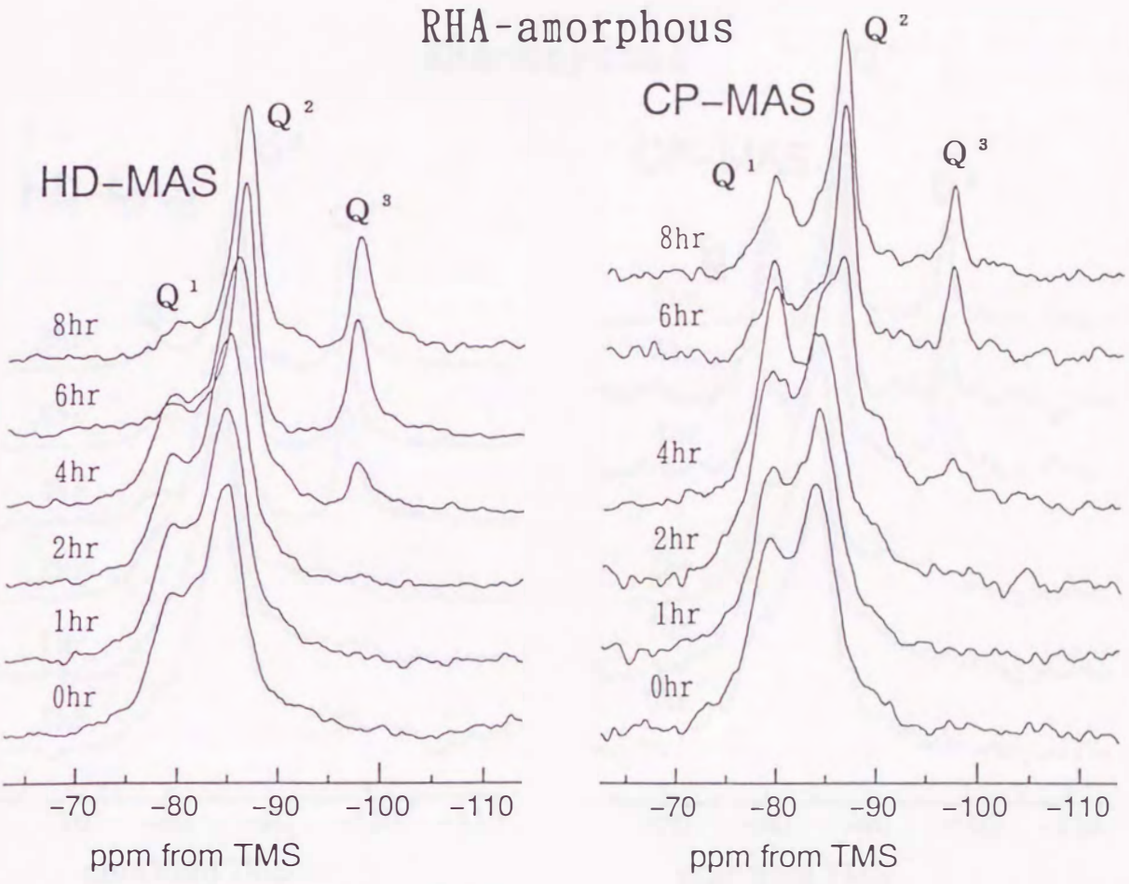

Figure 4.5 ^{29}Si HD-MAS and CP-MAS NMR spectra of the products hydrothermally synthesized from RHA-amorphous.

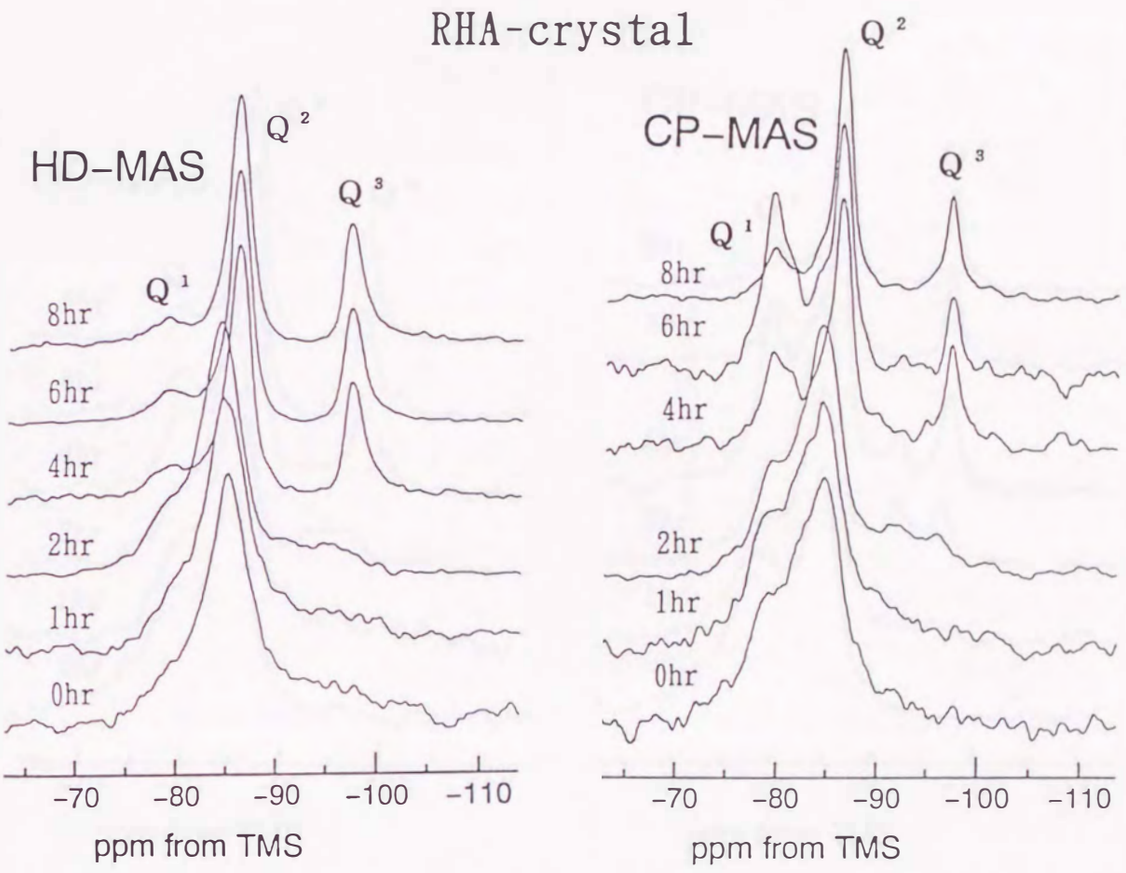

Figure 4.6 ^{29}Si HD-MAS and CP-MAS NMR spectra of the products hydrothermally synthesized from RHA-crystal.

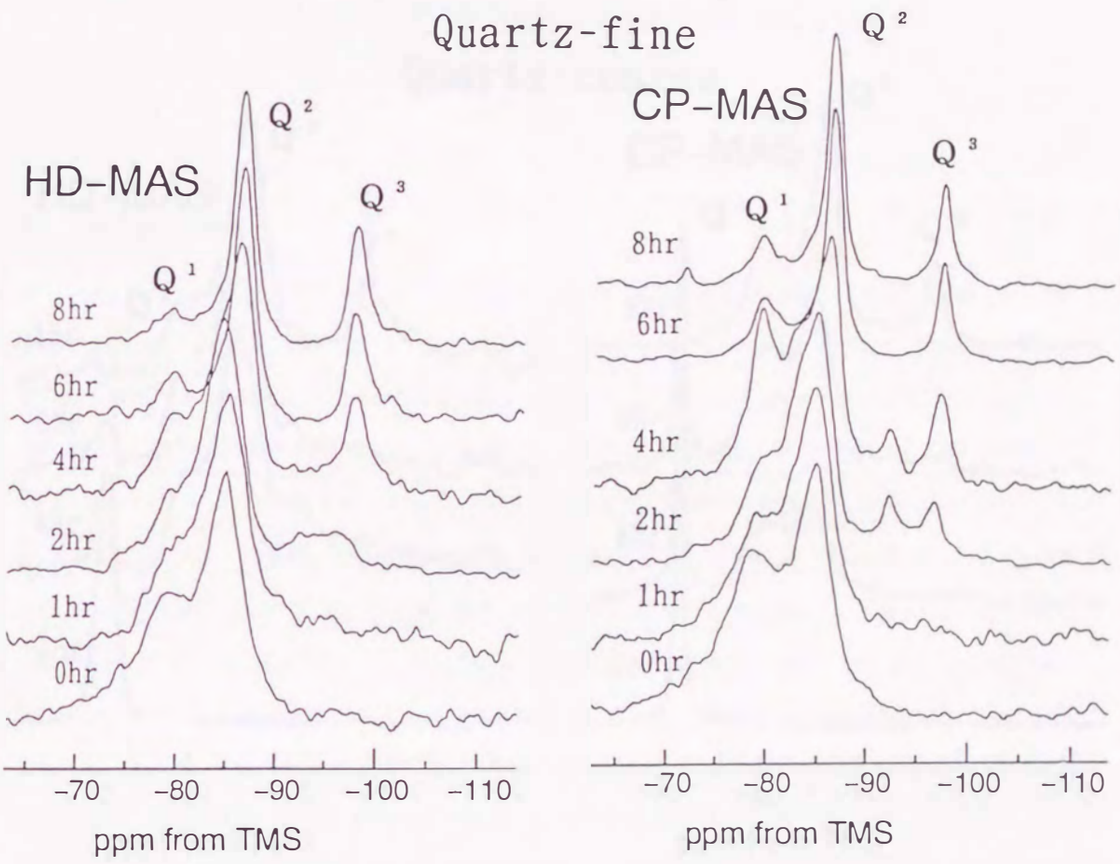

Figure 4.7 ^{29}Si HD-MAS and CP-MAS NMR spectra of the products hydrothermally synthesized from Quartz-fine.

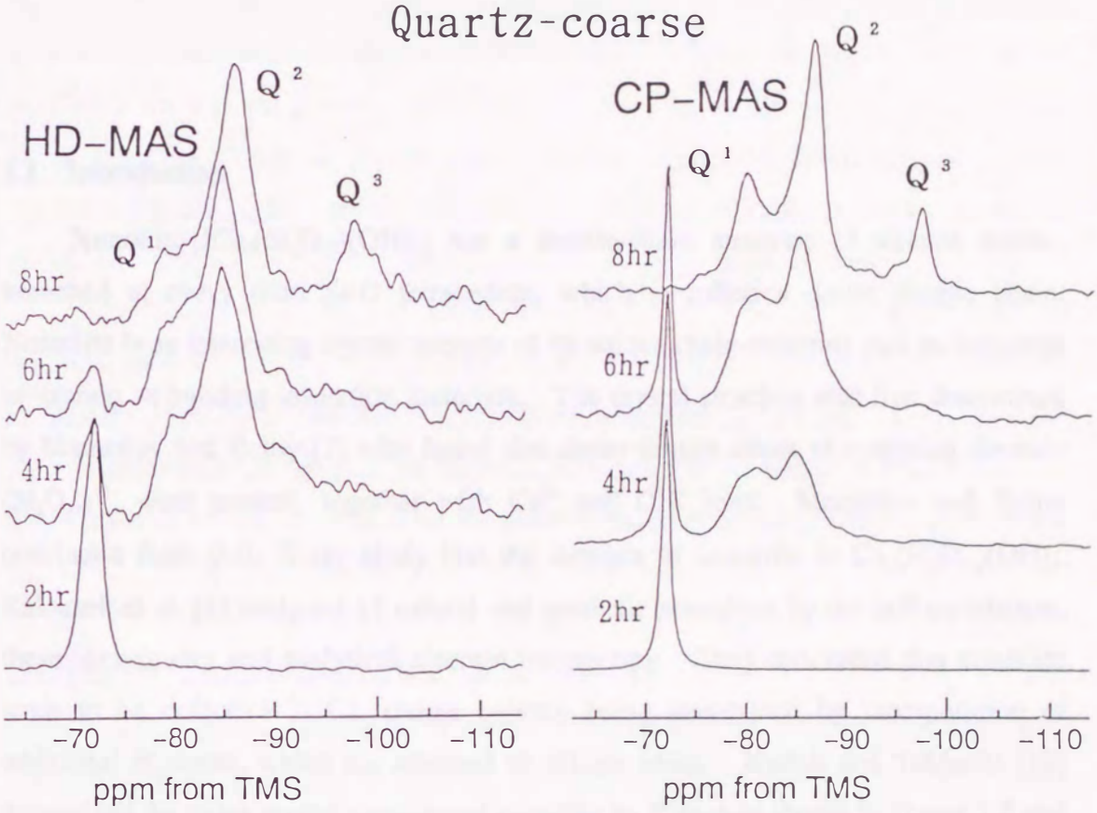

Figure 4.8 ^{29}Si HD-MAS and CP-MAS NMR spectra of the products hydrothermally synthesized from Quartz-fine.

Chapter 5

High Resolution ^{29}Si and ^{1}H MAS NMR Spectra of Natural and Synthetic Xonotlite Crystals

5.1 Introduction

Xonotlite [$Ca_6(Si_6O_{17})(OH)_2$] has a double-chain structure of silicate anions, branched at every third Si-O tetrahedron, which is called a dreier double chain. Xonotlite is an interesting crystal because of its unique chain-structure and its industrial utilization as building insulation materials. The crystal structure was first determined by Mamedov and Belov [7] who found that dreier double chain of empirical formula $(Si_6O_{17})^{12-}$ were present, together with Ca^{2+} and OH^- ions. Mamedov and Belov concluded from their X-ray study that the formula of xonotlite is $Ca_6(Si_6O_{17})(OH)_2$. Kalousek et al. [8] analyzed 15 natural and synthetic xonotlites by the cell parameters, thermogravimetry and analytical electron microscopy. They concluded that xonotlite tends to be defective in Ca, charge balance being maintained by incorporation of additional H atoms, which are attached to silicate anion. Kudoh and Takéuchi [10] determined the exact crystal structure of xonotlite by X-rays as shown in Figure 1.2 and discussed the polytypism of xonotlite.

The ^{29}Si MAS NMR of synthetic xonotlite has been reported by Lippmaa et al. [30], Bell et al. [37] and Cong et al. [46]. They reported the two signals at –86.8 ppm (Q^2) and –97.8 ppm (Q^3) with a 2:1 intensity ratio as shown in Figure 1.7, which reflected well the double chain structure of xonotlite with a 2:1 ratio of the contents of Q^2 and Q^3 groups. Grimmer and Wieker [49] first observed the ^{1}H wideline NMR of

synthetic xonotlite and determined the H types in xonotlite by analyzing the line shape. The ^{1}H MAS NMR of synthetic xonotlite was reported by Rosenberger et al. [50].

The preceding NMR studies of xonotlite have been only for synthetic xonotlite. The reported ^{29}Si MAS NMR signals of synthetic xonotlite were broad as shown in Figure 1.7. I also observed the ^{29}Si MAS NMR signals of only synthetic xonotlites, which were synthesized at 200 °C and 190 °C in Chapters 3 and 4, respectively. Xonotlites can be and are industrially synthesized at around 200 °C. However, the crystallinity of synthetic xonotlites heavily depends on the hydrothermal reaction temperature and tends to improve with increased temperature [8]. The synthetic xonotlites showed the poorer XRD patterns than those of the natural xonotlites [8]. When the crystallinity of the samples decreases, the MAS NMR signals become broader. Therefore, high resolution NMR signals will be obtained by using the natural xonotlites and the synthetic xonotlite synthesized at higher temperatures.

Rosenberger et al. [50] obtained the chemical shift of the ^{1}H MAS NMR of synthetic xonotlite, 2 ppm, but did not deconvolute the signal. Xonotlite has not only structural OH in the crystal but also molecular water and Si-OH [8]. Grimmer et al. [49] deconvoluted the ^{1}H wideline NMR signals of synthetic xonotlite and determined the H types in xonotlite. The wideline NMR signals are much broader than the MAS signals so that the deconvolution of wideline signals is more difficult than that of MAS signals. If the high resolution ^{1}H MAS NMR of xonotlite is obtained, H types in xonotlite can be determined much more quantitatively.

In this chapter, I prepared the natural xonotlite and the synthetic xonotlite with high crystallinity and tried to observe the high-resolution ^{29}Si and ^{1}H MAS NMR spectra. The xonotlite crystal structure is examined by these NMR signals. I first observed the splitting of the Q^2 signal into two signals with a 1:1 intensity ratio for both natural and synthetic xonotlites. The assignment of these two Q^2 signals is discussed based on the xonotlite structure determined by XRD. I first succeeded in the quantitative deconvolution of the ^{1}H MAS NMR signals into three signals. The signal assignment is established by comparison with the TG analysis results.

5.2 Experimental

5.2.1 Preparation of Xonotlites

The natural xonotlite was collected from Ohmi-machi, Keijoh-gun, Nihgata Prefecture, Japan. The synthetic xonotlite was hydrothermally synthesized at 250 °C for 60 h from CaO and silicic acid. The starting Ca/Si molar ratio was 1.0 and the water/solid ration was 40. CaO was prepared by heating reagent grade $CaCO_3$ at 1000°C for 4 hours. The silicic acid was amorphous silica of reagent grade with 20.8% ignition loss. The products were filtered and dried in a vacuum at 60°C for 2 days and then examined by XRD and TG (thermogravimetry). The TG was measured at the heating rate of 5°C/min with N_2 gas flowing at 100 ml/min.

5.2.2 NMR Measurement

NMR spectra were obtained using a Bruker AC200 (4.7 T) and a Bruker DSX300 (7.5 T). The ^{29}Si NMR was recorded using a Bruker AC200 (4.7 T) with a MAS rate of 3.25 kHz. The ^{29}Si high power decoupling (HD-MAS) spectra were obtained using a $\pi/4$ pulse (2 μs) with a repetition time of 1000 s and 128 pulses for the natural one and with that of 30 s and 1024 pulses for the synthetic one. The ^{29}Si cross polarization (CP-MAS) spectra were obtained with a repetition time of 20 s, a contact time of 4 ms and 1024 pulses. The ^{1}H NMR was acquired using an ordinary single-pulse sequence with a $\pi/2$ pulse (4.6 μs), a repetition time of 25 s and 16 pulses on a Bruker DSX300 (7.05 T) with a MAS rate of 12 kHz. The ^{29}Si chemical shift of 3-(trimethylsilyl)-propane sulfonic acid sodium salt (DSS) was 1.534 ppm [67] and the ^{1}H shift of water was 4.877 ppm [67].

5.3 Results and Discussion

5.3.1 Chemical Compositions and XRD

The results of the wet chemical analysis of the natural and synthetic xonotlites are summarized in Table 5.1. The XRD of natural and synthetic xonotlites are shown in Figure 5.1. According to their XRD patterns, the natural xonotlite did not contain any

mineral impurities and the synthetic one contained unreacted neither $Ca(OH)_2$ nor silica. The XRD patterns of both natural and synthetic xonotlites in Figure 5.1 are much sharper than those of xonotlites synthesized at 190 ℃ in Figures 4.1, 4.2, 4.3, and 4.4. This fact indicates that both natural and synthetic xonotlites are much highly crystalline.

5.3.2 ^{29}Si NMR Spectra

The HD-MAS and CP-MAS spectra of natural xonotlite are shown in Figure 5.2. Only the Q^2 and Q^3 signals were observed while Q^1 was not detected. Q^2 was clearly split with an intensity of 1:1, contrary to the previous reports [30, 37, 46]. The HD-MAS and CP-MAS spectra of synthetic xonotlite are shown in Figure 5.3. The chemical shifts of the natural and synthetic crystals showed almost the same values. The chemical shifts and relative intensities are summarized in Table 5.2. The Q^1 signal is clear and enhanced particularly in the CP-MAS spectrum. The Q^2 signal was split like natural one. The NMR signals of the synthetic xonotlite are broader than those of the natural one. This indicates the higher crystallinity of the natural one than the synthetic one.

5.3.3 Q^1 Site of Synthetic Xonotlite

Q^1 is an end site of the silicate anion chain and a defect in the xonotlite crystals. This was not observed for natural xonotlite with higher crystallinity. The enhancement of the Q^1 signal by CP indicates the existence of protons such as Si-OH near Q^1 [54].

5.3.4 Splitting of Q^2 Signals

The two signals of Q^2 at –86.3 ppm and –87.1 ppm were observed for both the natural and synthetic xonotlites and their intensity ratio was near 1:1, which indicates the two signals are caused not by contamination but by its proper crystal structure. While only one Q^2 signal was observed at –86.8 ppm in the previous studies [30, 37, 46] and its signal was much broader than our signals. The specimens of the previous studies [30, 37, 46] were synthetic and they showed a large amount of Q^1 signal, which

indicates poor crystallinity of the specimens [54]. It might be the reason why the split of Q^2 signal could not be detected.

According to the analysis of the xonotlite crystal structure by Kudoh et al. [10], the two Q^2 sites have different mean Si–O bond lengths and mean Si–O–Si bond angles as shown in Figure 5.4.

Wollastonite [β-$CaSiO_3$], which has dreier single chains similar to the dreier double chains of xonotlite, was expected to show three different ^{29}Si NMR signals according to the crystal structure [58]. Wollastonite has three different Si sites of Q^2 with mean Si-O bond lengths of 1.623, 1.621 and 1.633 Å and mean Si-O-Si angles of 144.95, 145.32 and 139.72° [68, 69]. Sebald et al. [68] first observed three different signals of natural wollastonite at –87.7, –88.9 and –89.3 ppm with a signal intensity ration of 1:1:1. Sebald et al. discussed the assignment of these signals to the three Si sites. They assigned the signal at –87.7 ppm to the Si site with mean Si-O bond lengths of 1.633 Å and mean Si-O-Si angles of 139.72°. However they concluded that the other two signals with a chemical shift difference of only 0.4 ppm cannot be assigned by the empirical correlations between a chemical shift and simple crystal structure criteria.

The Q^2_H and Q^2_L in Figures 5.2 and 5.3 must correspond to Si(1) and Si(2) in Figure 5.4. The ^{29}Si signal shifts toward the lower frequency with a decrease in the mean Si–O bond lengths [70] or with an increase in the mean Si–O–Si bond angles [71]. According to the above empirical correlations, the signal at –87.1 ppm is ascribed to the Si site having the shorter mean Si–O bond length and the larger mean Si–O–Si bond angle. As shown in Figure 5.4, Si(1) has a shorter mean Si–O bond length while Si(2) has a larger mean Si–O–Si bond angle. Consequently, it is difficult to assign these two signals using the above empirical correlations.

5.3.5 ^1H MAS NMR

Figure 5.5 shows the ^1H MAS NMR spectra of the natural and synthetic xonotlites. A sharp signal at 2.2 ppm with a shoulder and a broad signal at 5.0 ppm were observed for both samples. The signals were deconvoluted into three lines at

2.19, 1.86 and 5.26 ppm. The relative intensities of these signals were summarized in Table 5.3.

5.3.6 Assignment of ^{1}H MAS NMR Signals

Xonotlite has not only structural OH in the crystal but also molecular water and Si-OH [8]. The TG losses from the specimens were analyzed and could be divided into three parts, room temperature – 200 °C – 700 °C – 850 °C. The ratios of the TG losses in each temperature range were summarized in Table 5.4. These results are in good agreement with the ^{1}H NMR signal intensities if the TG losses in the ranges of room temperature – 200 °C – 700 °C – 850 °C correspond to the signals at 5.16 ppm, 1.86 ppm and 2.19 ppm, respectively. Moreover the signal at 5.26 ppm disappeared by vacuum-drying at 80 °C for 1 d. The chemical shift of 1.86 ppm is very near to 1.7 ppm assigned to isolated (non-H-bonded) Si-OH of silica gel by Bronnimann et al [72]. Kudoh et al.[3] estimated the location of structural OH at the central Ca–O among the four Q^2 units of the double chain [10]. Rassem [52] summarized the ^{1}H NMR chemical shifts of calcium silicate hydrates and assigned the OH of xonotlite (2.0 ppm) [46] as Ca-OH. Consequently, the signals at 5.26, 1.86 and 2.19 ppm can be assigned to the molecular water, Si-OH and structural Ca-OH, respectively.

5.4 Conclusions

The high resolution ^{29}Si and ^{1}H MAS NMR spectra of natural and synthetic xonotlites with high crystallinity were observed. The xonotlite structure was examined by these NMR signals. The results are as follows.

1) The Q^1 site, which is a defect of xonotlite silicate chains, was observed only for the synthetic xonotlite. ^{1}H nuclei are localized near Q^1 sites because the Q^1 signal was enhanced by the CP.

2) It was first observed that two ^{29}Si-NMR signals (–86.3, –87.1 ppm) of Q^2 of the natural and synthetic xonotlites were clearly split. This result indicates that Q^2 has two crystallographically different sites, which is in accord with the crystal structure study of Kudoh et al [10].

3) ^{1}H MAS NMR spectra of the natural and synthetic xonotlites show a sharp signal at 2.2 ppm with a shoulder and a broad signal at 5.0 ppm. The signals can be deconvoluted into three lines at 2.19, 1.86 and 5.26 ppm. The TG losses from the specimens were analyzed and divided into three parts, room temperature – 200 °C – 700 °C – 850 °C. The ratios of the TG losses in each temperature range are in good agreement with the ^{1}H NMR signal intensities. Therefore, the signals at 2.19, 1.86 and 5.26 ppm are assigned to structural Ca-OH, Si-OH and molecular water, respectively.

Table 5.1 Chemical compositions of natural and synthetic xonotlites.

Sample	Ig. Loss	SiO_2	Al_2O_3	Fe_2O_3	TiO_2	CaO	Na_2O	K_2O	MnO	total
Natural	3.18	50.80	0.38	0.05	tr	44.70	0.78	0.02	0.01	99.92
Synthetic	3.05	49.51	0.36	0.07	0.01	45.54	0.76	0.03	tr	99.33

Table 5.2 Relative intensities (%) of Q^1, Q^2 and Q^3 of ^{29}Si HD-MAS and CP-MAS spectra of natural and synthetic xonotlites.

		Q^1	Q^2_H	Q^2_L	Q^3
Chemical shift (ppm from TMS)		-79.6	-86.3	-87.1	-97.5
Natural	HD	0	39	29	32
	CP	0	37	34	29
Synthetic	HD	4	36	30	30
	CP	17	43	21	19

Q^2_H, Q^2_L: higher- and lower-frequency signals of Q^2.

Table 5.3 Relative intensities (%) of ^{1}H MAS NMR signals of natural and synthetic xonotlites.

Chemical shift (ppm from TMS)	5.16	2.19	1.86
Natural	9	73	18
Synthetic	11	65	24

Table 5.4 Ratios (%) of TG losses in three temperature ranges of natural and synthetic xonotlites.

	room temperature – 200 °C	200 °C – 700 °C	700 °C – 850 °C
Natural	10	17	73
Synthetic	10	24	66

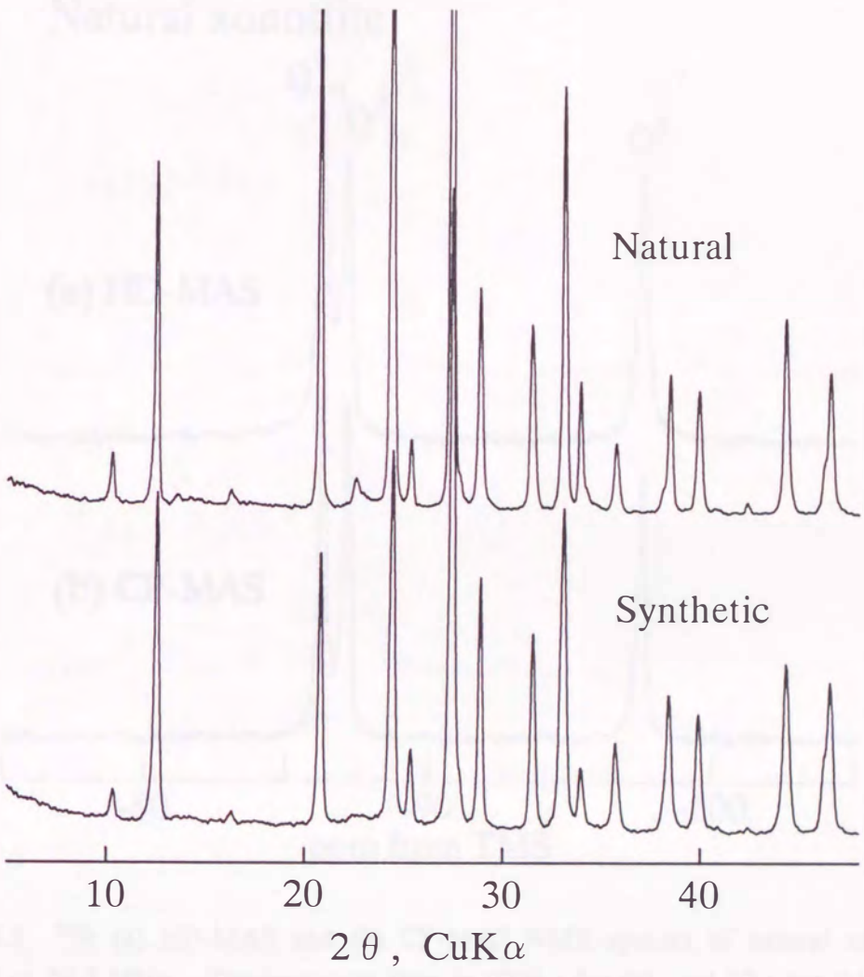

Figure 5.1 XRD patterns of the natural and synthetic xonotlites.

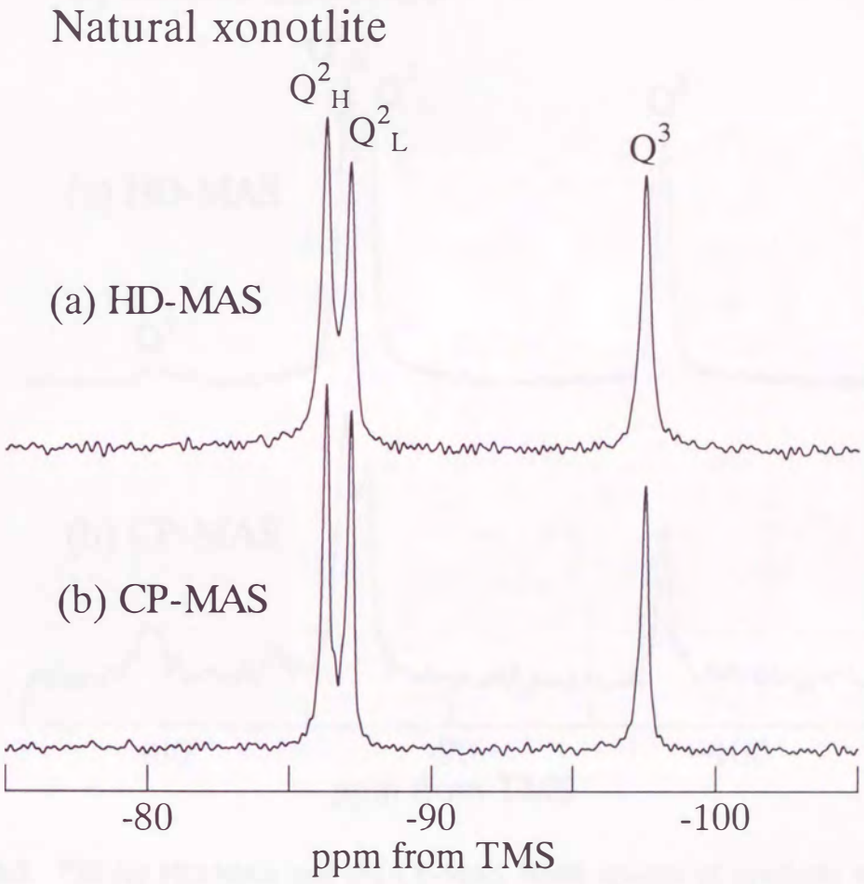

Figure 5.2 ^{29}Si (a) HD-MAS and (b) CP-MAS NMR spectra of natural xonotlite measured at 39.7 MHz. The repetition time is 1000 s for (a), and 20 s for (b). The number of pulses, the spinning rate of the sample, and the line broadening factor are 128, 3.25 kHz, and 1 Hz, respectively. The contact time of cross polarization is 4 ms for (b).

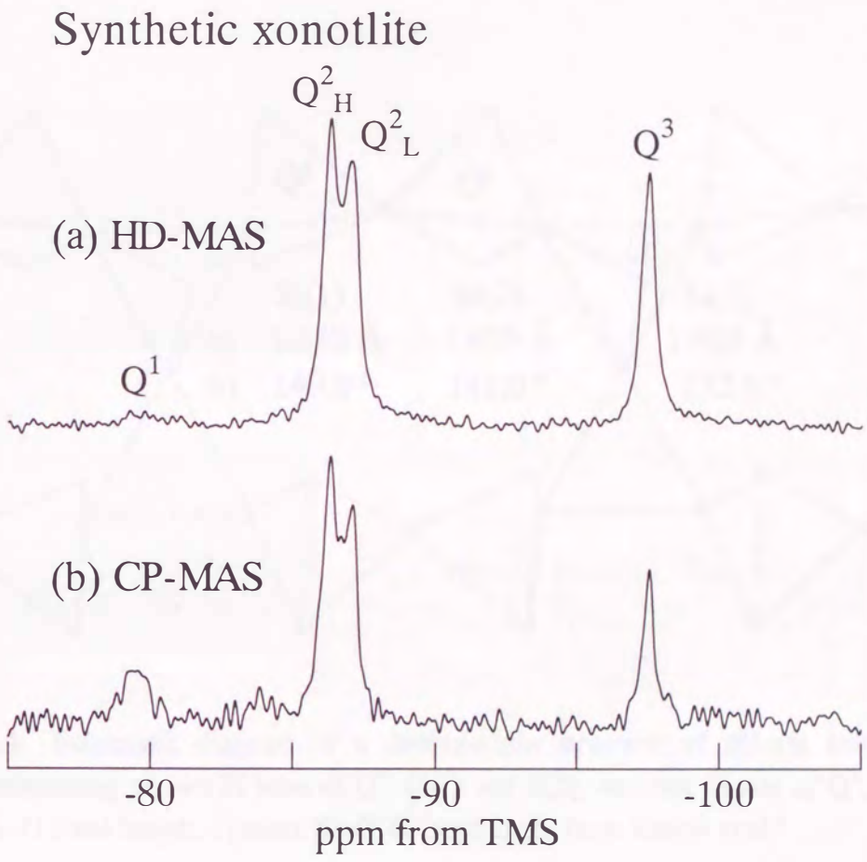

Figure 5.3 ^{29}Si (a) HD-MAS and (b) CP-MAS NMR spectra of synthetic xonotlite measured at 39.7 MHz. The repetition time and the number of pulses are 30 s and 4096 for (a), and 20 s and 1024 for (b). The spinning rate of the sample and the line broadening factor are 3.25 Hz and 1 Hz, respectively. The contact time of cross polarization is 4 ms for (b).

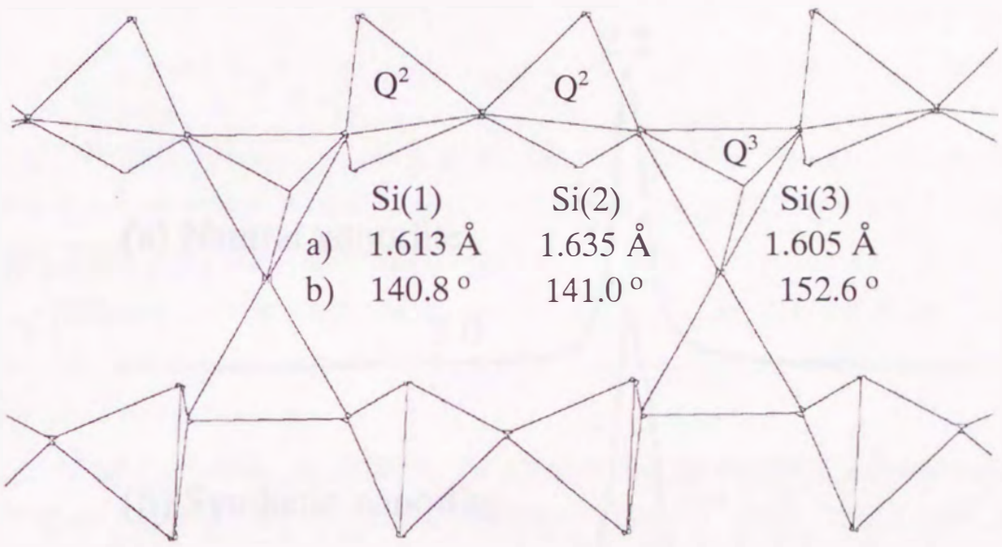

Figure 5.4 Schematic diagram of a double-chain structure of silicate anions in xonotlite consisting of two Si sites of Q^2, Si(1) and S(2), and one Si site of Q^3, Si(3). a) mean Si–O bond length, b) mean Si–O–Si bond angle from Kudoh et al.[3]

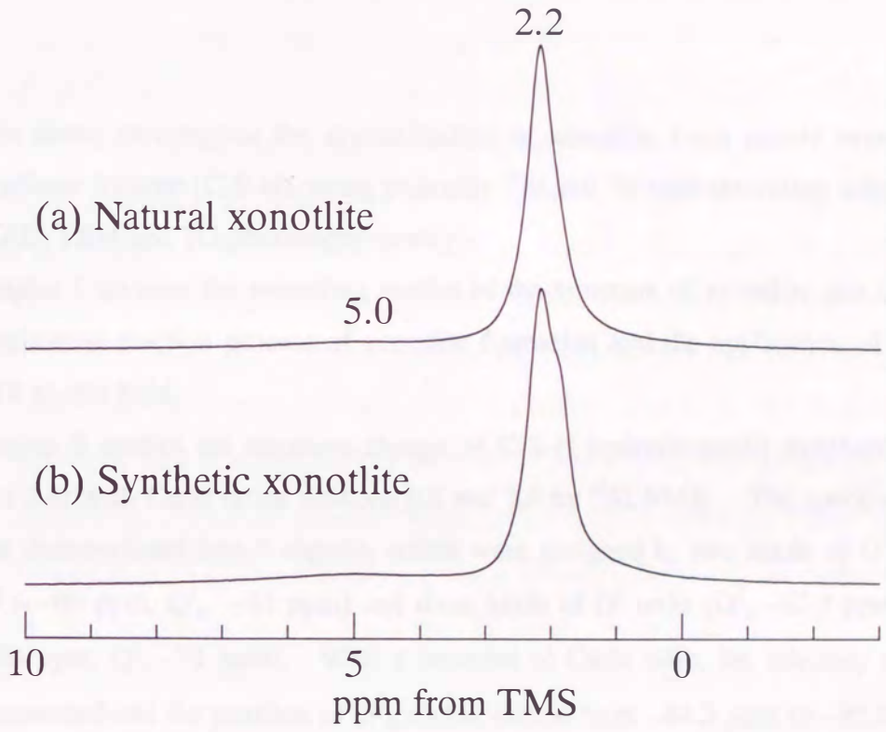

Figure 5.5 ^{1}H MAS-NMR spectra of natural and synthetic xonotlite measured at 300 MHz. The ordinary single-pulse sequence is used. The repetition time, the number of pulses, the spinning rate of the sample, and the line broadening factor are 20 s, 16, 12 kHz, and 0 Hz, respectively.

Chapter 6

Summary

This thesis investigates the crystallization of xonotlite from poorly crystalline calcium silicate hydrate (C-S-H), using primarily ^{29}Si and ^{1}H high-resolution solid-state NMR, XRD, TEM and TG (thermogravimetry).

Chapter 1 reviews the preceding studies of the structure of xonotlite and C-S-H, the hydrothermal reaction process of xonotlite formation and the application of solid-state NMR to this field.

Chapter 2 studies the structure change of C-S-H hydrothermally synthesized at 130°C for 2 hr with Ca/Si ratios between 0.6 and 2.0 by ^{29}Si NMR. The spectra of C-S-H were deconvoluted into 5 signals, which were assigned to two kinds of Q^1 units (Q^1_H –79 ~ –80 ppm, Q^1_L –81 ppm) and three kinds of Q^2 units (Q^2_H –82.5 ppm, Q^2_M –84 ~ –86 ppm, Q^2_L –91 ppm). With a decrease of Ca/Si ratio, the intensity of Q^1_H signals decreased and the position of Q^2_M signal shifted from –84.2 ppm to –85.6 ppm. The Q^2_M signal at –85.6 ppm and the Q^2_H signal at –82.5 ppm are assigned to the paired Q^2 and the bridging Q^2 with OH, respectively. The C-S-H phase with Ca/Si of 1.5 was treated by H-type ion exchange resin at room temperature and changed to C-S-H phases with lower Ca/Si ratios. It was found out that the Q^1 units decrease in a short time (2 min) by this treatment. To explain this abrupt decrease of Q^1, the separation model of silicate anions by insertion of Ca^{2+} ions was proposed. The Q^1_L signal at –81 ppm was assigned to Q^1 units separated by Ca^{2+} ions.

Chapter 3 studies the formation process of xonotlite from C-S-H, using TEM observation, the degree of formation (α) evaluated by thermogravimetry, and ^{29}Si solid-state NMR. The TEM observation confirms that C-S-H prepared hydrothermally shows homogeneous foil-like morphology and the nucleation of xonotlite and its

one-dimensional crystal growth occurs in C-S-H. The analysis of the formation rate on the nucleation and growth model suggests that the one-dimensional phase-boundary controlled growth be in accord with the TEM observation. The apparent activation energy of nucleation and that of growth were almost the same values, 118 and 111 $kJ \cdot mol^{-1}$, respectively. The chemical shift of ^{29}Si NMR of middle groups Q^2 of C-S-H changed from –84.3 to –85.6 ppm during the induction period of xonotlite formation, which suggests some of Q^2 became well bonded to Ca–O layer and is the origin of nuclei of xonotlite crystals. The mean chain length of silicate anions was estimated from Q^2/Q^1 and $(Q^2+Q^3)/Q^1$ intensity ratios. The mean silicate chain length decreased during the induction period and increased with formation of xonotlite.

Chapter 4 studies the influence of the siliceous materials on the xonotlite formation using 4 kinds of siliceous materials. The siliceous materials were two kinds of rice husk ash with different crystallinity (RHA-amorphous, RHA-crystal) and two kinds of silica sand with different particle size distribution (Quartz-fine, Quartz-coarse). The order of the rate of dissolution of siliceous materials was considered in terms of solubility and specific surface area as follows; RHA-amorphous $\gg$ RHA-crystal > Quartz-fine $\gg$Quartz-coarse. The reaction process was highly dependent on the rate of dissolution of siliceous materials. The products formed in the early stage of the reaction vary with siliceous materials and determine the reaction process. The C-S-H formed from RHA-amorphous has relatively sharp XRD peaks and NMR signals of Q^1 and Q^2. This C-S-H directly changes to xonotlite. The C-S-H formed from RHA-crystal and Quartz-fine has a broad XRD pattern and a broad Q^2 signal between –90 and –100 ppm in addition to the Q^1 and Q^2 signals observed in the C-S-H from RHA-amorphous. This C-S-H easily changed to tobermorite and next xonotlite is formed. α-C_2SH is formed from Quartz-coarse and changed to C-S-H and to xonotlite.

Chapter 5 studies the structure of xonotlite by the high resolution ^{29}Si and ^{1}H MAS NMR spectra of natural and synthetic xonotlites. The Q^1 site, which is a defect of xonotlite silicate chains, was observed only for the synthetic xonotlite. It was first observed that two ^{29}Si-NMR signals (–86.3, –87.1 ppm) of Q^2 of the natural and synthetic xonotlites were clearly split. This result indicates that Q^2 has two crystallographically different sites, which is in accord with the crystal structure study of

Kudoh et al [10]. ^{1}H MAS NMR spectra of the natural and synthetic xonotlites show a sharp signal at 2.2 ppm with a shoulder and a broad signal at 5.0 ppm. The signals can be deconvoluted into three lines at 2.19, 1.86 and 5.26 ppm, which are assigned to structural Ca-OH, Si-OH and molecular water, respectively.

References

1. H.F.W. Taylor, "The Chemistry of Cements vol.1" ed by H.F.W. Taylor, Academic Press, London (1964), Chap. 5.
2. T. Mitsuda, "Suinetsukagaku Handobukku", ed by S. Somiya, N. Yamasaki, S. Hirano, M. Yoshimura, Gihodo Shuppan, Tokyo (1997), II-2.2.
3. S. Nagai, *Z. Anorg. Chem.*, **206**, 177 (1932).
4. S. Nagai, *Z. Anorg. Chem.*, **207**, 321 (1932).
5. L. Heller, *Proc. 3rd Int. Symp. Chemistry of Cement, London 1952*, 237 (1954).
6. L.S. Dent and H.F.W. Taylor, *Acta. Cryst.*, **9**, 1002 (1956).
7. Kh.S. Mamedov and N.V. Belov, *Dokl. Akad. Nauk. S.S.S.R*, **104**, 615 (1955).
8. L. Kalousek, T. Mitsuda, and H.F.W. Taylor, *Cement Concr. Res.*, **7**, 305 (1977).
9. J.A. Gard, *Nature*, **211**, 1078 (1966).
10. Y. Kudoh and Y. Takéuchi, *Miner. J.*, **9**, 349 (1979).
11. Y. Mitsuda, J. Saito, and E. Hattori, *Proc. Int. Symp. Hydrothermal Reaction, Yokohama, 1982*, 823 (1983).
12. S.A.S. El-Hemaly, T. Mitsuda, and H.F.W. Taylor, *Cement Concr. Res.*, **7**, 429 (1977).
13. R. Kondo, *Proc. Symp. Autoclaved Calcium Silicate Building Products, London, 1965*, 92 (1967).
14. C.F. Chan, M. Sakiyama, and T. Mitsuda, *Cement Concr. Res.*, 8, 1 (1978).
15. T. Ishii, C.F. Chan, and T. Mitsuda, *Semento Gizyutsu Nenpo*, 32, 75 (1978).
16. T. Mitsuda, S. Kobayakawa, and H. Toraya, *Proc. 8th Int. Congress Chemistry Cement, Rio de Janeiro, 1986*, **3**. 173 (1986).
17. H.F.W. Taylor, *J. Am. Ceram. Soc.*, **69**, 464 (1986).
18. H.F.W. Taylor, "Cement Chemistry", Academic Press, London (1990), Chap. 5.
19. H.F.W. Taylor, *J. Chem. Soc.*, **1950**, 3682.
20. H.F.W. Taylor, *Proc. Int. 5th Int. Symp. Chem. Cement, Tokyo,* **II**, 1 (1968).

21. J.D. Bernal, *Proc. Int. 3rd Int. Symp. Chem. Cement, London*, 216 (1952).
22. J.A. Gard and H.F.W. Taylor, *Cement Concr. Res.*, 6, 667 (1976).
23. J.A Pople, W.G. Schneider, and H.J. Bernstein, "High-resolution Nuclear Magnetic Resonance", McGraw-Hill Book Company, New York (1959).
24. Japan Chemical Society, "Zikken-kagaku-koza 5 NMR ", Maruzen, Tokyo (1991).
25. A. Abragam, "Principles of Nuclear Magnetism", Oxford University Press, Oxford (1961).
26. C.P. Slichter, "Principles of Magnetic Resonance" 3rd ed, Springer-Verlag, Berlin (1990).
27. M. Mehring, "High Resolution NMR Spectroscopy in Solids", Springer-Verlag, Berlin (1976).
28. B.C. Gerstein and C. R. Dybowski, "Transient Techniques in NMR of Solids", Academic Press Inc., Orlando, (1985).
29. A.-R. Grimmer and B. Blümich, "Introduction to Solid-State NMR" in "NMR 30 Solid-State NMR I Methods", ed by B. Blümich, Springer-Verlag, Berlin (1994).
30. Lippmaa, M. Mägi, A. Samoson, G. Engelhardt, and A.-R. Grimmer, *J. Am. Chem. Soc.*, **102**, 4889 (1980).
31. M. Mägi, Lippmaa, A. Samoson, G. Engelhardt, and A.-R. Grimmer, *J. Phys. Chem.*, **88**, 1518 (1984).
32. G. Engelhardt and D. Michel, "High-Resolution Solid-State NMR of Silicates and Zeolites", John Wiley & Sons, Chichester (1987).
33. E. Lippmaa, M. Mägi, M. Tarmak, W. Wieker, and A.-R. Grimmer, *Cem. Conc. Res.*, **12**, 597 (1982).
34. W. Wieker, A.-R. Grimmer, A. Winkler, M. Mägi, M. Tarmak, and E. Lippmaa, *Cem. Conc. Res.*, **12**, 333 (1982).
35. H. Stande, A.-R. Grimmer, G. Engelhardt, M. Mägi, and E. Lippmaa, *Z. Anorg. Allg. Chem.*, **528**, 147 (1985).
36. M. Grutzeck, A. Benesi, and B. Fanning, *J. Am. Ceram. Soc.*, **72**, 665 (1989).
37. G.M.M. Bell, J. Bensted, F.P. Glasser, E.E. Lachowski, D.R. Roberts, and M.J. Taylor, *Adv. Cement Res.*, **3**, 23 (1990).
38. H. Sato and M. Grutzeck, *Mat. Res. Soc. Symp. Proc.*, **245**, 235 (1992).

39. P. Colombet and A.-R. Grimmer, "Application of NMR Spectroscopy to Cement Science", Gordon & Breach Science Publishers (1994).
40. A.R. Brough, C.M. Dobson, I.G. Richardson, and G.W. Groves, *J. Am. Ceram. Soc.*, **77**, 593 (1994).
41. T. Mitsuda, H. Toraya, Y. Okada, and M. Shimoda, *Ceramic Transaction*, **5**, 206, (1988).
42. Y. Okada, H. Ishida, and T. Mitsuda, *J. Am. Ceram. Soc.*, **77**, 765 (1994).
43. Y. Okada, N. Isu, T. Masuda, and H. Ishida, *J. Ceram. Soc. Jap.*, **102**, 1148 (1994).
44. Y. Okada, Ph. D. Thesis, Nagoya Institute of Technology, Nagoya, Japan, 1994.
45. X. Cong and R.J. Kirkpatrick, *Adv. Cement Res.*, **7**, 103 (1995).
46. X. Cong and R.J. Kirkpatrick, *Adv. Cem. Based Mater.*, **3**, 133 (1996).
47. X. Cong and R.J. Kirkpatrick, *Adv. Cem. Based Mater.*, **3**, 144 (1996).
48. X. Cong, Ph. D. Thesis, University of Illinois, Urbana-Champaign, U.S.A., 1994.
49. A.-R. Grimmer and W. Wieker, *Z. Allg. Anorg. Chem.*, **384**, 34 (1971).
50. H. Rosenberger and A.-R. Grimmer, *Z. Allg. Anorg. Chem.*, **448**, 11 (1979).
51. D. Heidemann, "Application of NMR Spectroscopy to Cement Science", ed by P. Colombet, A.-R. Grimmer, Gordon & Breach Science Publishers (1994), Chap. 5.
52. R. Rassem, H. Zanni-Théveneau, D. Heidemann, and A.-R. Grimmer, *Cement Concr. Res.*, **23**, 169 (1993).
53. H. Noma and H. Yamada, *Gypsum & Lime*, **231**, 27 (1991).
54. H. Noma, T. Yokoyama, Y. Adachi, and Y. Yamada, *Gypsum & Lime*, **251**, 18 (1994).
55. H. Noma, Y. Adachi, H. Yamada, Y. Matsuda, and T. Yokoyama, *Proc. 2nd Int'l. Meeting Pacific Rim Ceram. Soc., Cairns, Australia, 1996*, (in press).
56. T. Nishino and H. Noma, *Proc. 46th Meeting Cement Assoc. Jap.*, p. 176 (1992).
57. T. Nishino and T. Sakurai, *Proc. 88th Meeting Jap. Soc. Gypsum & Lime*, p. 26 (1994).
58. N. Janes and E. Oldfield, *J. Am. Chem. Soc.*, **107**, 6769 (1985).
59. S.F. Hulbert, *J. Brit. Ceram. Soc.*, **6** , 11 (1969) .
60. D.T. Hayhurst and L.B. Sand, "Molecular Sieves II", ed by J.R.Katzer, Am. Chem. Soc. Symp. Series, No.40 (1977), p.219.

61. P.W. Brown, J. Pommershein and G. Frohnsdorff, *Cem. Concr. Res.*, **15**, 35 (1985).
62. H. Noma, N. Inoue, H. Yamada, and N. Hara, *Rep. Kyushu Nat. Res. Inst.*, **52**, 14 (1994).
63. N. Hara, H. Yamada, K. Inoue, S. Tsunematsu, and H. Noma, *Proc. 3rd Int. Conf. Use of Fly Ash, Silica Fume, Slag & Natural Pozzolans in Concrete*, 499 (1989).
64. H.F.W. Taylor, *Mineral. Mag.*, **32**, 110 (1959).
65. W.L. Marshall, *Geochim. Cosmochim. Acta.*, **44**, 907 (1980).
66. D.F. Weill and Y. Bottinga, *Contr. Mineral. & Petrol.*, **25** 125 (1970).
67. S. Hayashi and K. Hayamizu, *Bull. Chem. Soc. Jpn.*, **64**, 685 (1991).
68. A. Sebald, L.H. Merwin, W.A. Dollase, and F. Seifert, *Phys. Chem. Miner.*, **7**, 9 (1990).
69. Y. Ohashi and L.W. Finger, *Am. Mineral.*, **63**, 274 (1978) .
70. A.-R. Grimmer and R. Radeglia, *Chem. Phys. Lett.*, **106**, 262, (1984).
71. J.V. Smith and C.S. Blackwell, *Nature (London)*, **308**, 521 (1984).
72. C.E. Bronnimann, R.C. Zeigler, and G.E. Maciel, *J. Am. Chem. Soc.*, **110**, 2023 (1988).

Acknowledgments

I wish to express my sincere thanks to Prof. Yoshihisa Matsuda and Associate Prof. Takushi Yokoyama for their kind guidance and valuable discussions throughout this study. Prof. Matsuda kindly gave me a chance to study in his laboratory. Associate Prof. Yokoyama suggested to me an application of solid-state NMR to my study. I appreciate Prof. Shinichi Ishiguro for reviewing this thesis. I thank Dr. Yoshihiro Okaue and Dr. Takahiko Kojima for their valuable suggestion to this study.

I would like to thank the staff of Kyushu National Industrial Research Institute, KNIRI. Mr. Hideo Yamada, head of Environment and Materials Sec., gave me continuous support throughout this study and important suggestions particularly to reaction mechanism. Dr. Yoshio Adachi kindly introduced me to solid-state NMR, and taught me its practical measurements and fundamental theories. Dr. Naomichi Hara, director of Inorganic Materials Dept., and Mr. Norihiro Inoue introduced me to cement chemistry and hydrothermal synthesis of calcium silicate hydrates. I thank Dr. Kazuhiko Jinnai, director general of KNIRI, Dr. Hiroshi Tateyama, Dr. Akiko Mori, Mr. Kozo Inoue, Mr. Shuji Tsunematsu and Dr. Satoshi Nishimura for their encouragement.

I am indebted to Prof. Tadashi Nishino, Musashi Institute of Technology, for his advice on H-type ion exchange resin treatment of C-S-H. I wish to thank Emeritus Prof. Takeshi Mitsuda, Nagoya Institute of Technology, for helpful discussions on formation mechanism and crystal structure of calcium silicate hydrates. I also wish to thank Dr. Yoshihiko Okada, Chichibu Onoda Cement Corp., for his encouragement and suggestions on solid-state NMR of calcium silicate hydrates. I am grateful to Prof. Kazuyori Urabe, Ryukoku University, for his helpful suggestion on the crystal structure of calcium silicate hydrates. I thank Dr. Shigenobu Hayashi, National Institute of Materials and Chemistry Research, for his valuable advice on solid-state NMR measurements. Many thanks are due to Prof. Seishi Goto, Yamaguchi University, for his encouragement.

Finally, I would like to thank my wife, Yasumi, for her continuous encouragement and support. Last but not least, I thank my mother, Sayoko, for her endless encouragement.

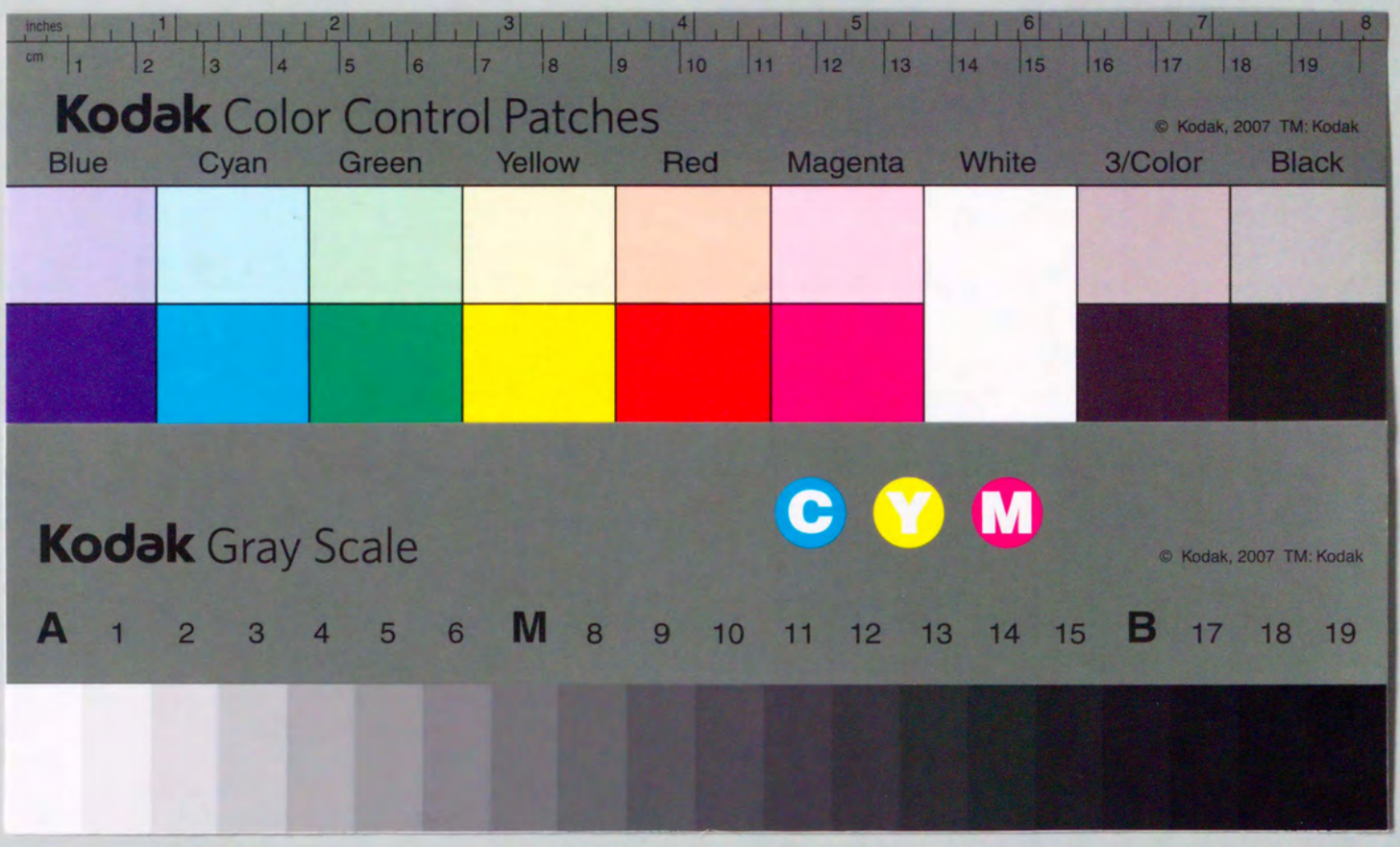
inches 1 2 3 4 5 6 7 8
cm 1 2 3 4 5 6 7 8 9 10 11 12 13 14 15 16 17 18 19
Kodak Color Control Patches
© Kodak, 2007 TM: Kodak
Blue Cyan Green Yellow Red Magenta White 3/Color Black
Kodak Gray Scale
C Y M
© Kodak, 2007 TM: Kodak
A 1 2 3 4 5 6 M 8 9 10 11 12 13 14 15 B 17 18 19